Journal of Composite Materials, **36**, 1825-1858 (2002)

Observations of Fiber Fracture and Interfacial Debonding Phenomena Using the Fragmentation Test in Single Fiber Composites

Ben W. Kim*
Structural Design & Development Branch, Air Vehicle Directorate
Air Force Research Laboratory, Wright-Patterson Air Force Base, Ohio, USA

John A. Nairn
Dept. of Materials Science & Engineering, University of Utah, Salt Lake City, Utah, USA

ABSTRACT

Fiber-reinforced polymer composites are being studied for many applications because of their potential for outstanding mechanical properties. To be used in new applications, composites have to be more fully understood. The fiber, the matrix, and the fiber/matrix interface are the building blocks that need study. This research has concentrated on the interface where debonds, or damage need to be studied more thoroughly. The experimental work here focused on the fragmentation test. The specimens used were AS4-carbon/Epoxy and E-glass/Epoxy composites. The fragmentation process was continuously monitored with careful attention to debonding at each break and debonding growth at higher strain as a function of applied tensile strain. Photoelastic birefringence patterns in the specimen were observed in more detail than ever to accurately monitor interfacial debonding and damage. The fiber fracture and the debonding length between the fiber and the matrix were measured only by visual observation using the photoelastic patterns rather than the Laser Raman Spectroscopy (LRS) which has usually been used in measuring interfacial debonding length or damage. This visual measurement technique provides the much simpler and more precise method than traditional LRS in measuring the fiber fracture and the interfacial damage in fiber-embedded composites. From the experimental data of fiber breaks and interfacial debond length, the interfacial toughness between the fiber and the matrix was analyzed for each composite system using the energy method. The interfacial debond energy, Γ_d, of AS4-Carbon/Epoxy was 220 J/m^2 and 130 J/m^2 for instantaneous debond and whole debond, respectively. For E-glass/Epoxy, Γ_d was obtained as 105 J/m^2 and 98 J/m^2 for instantaneous debond and whole debond, respectively.

Keywords: Single fiber composites, fragmentation test, fiber fracture, interfacial debonding, photoelastic birefringence, epoxy, AS4-carbon fiber, E-glass fiber, energy method

INTRODUCTION

Fiber-reinforced polymer composites are being studied as advanced materials for many areas. Many applications are considered because of their potential for outstanding mechanical properties. Fiber-reinforced composites are made of high-modulus fibers and relatively ductile polymer matrices. Fibers and polymeric matrices produce excellent mechanical properties when they are combined together. As a result, the composites have the high strength and modulus similar to that of the fibers and the lightweight and the chemical resistance of the polymeric matrix. Before these composites can be used in real products, a better understanding of their mechanical properties is needed. Therefore, some mechanical phenomena should be fully studied. The important checkpoints are the fiber, the matrix, and the fiber/matrix interface. If the bonding between two materials is unstable, and/or there is some damage at the interface, composites cannot be used properly with the advantage of excellent mechanical properties. Consequently, studying interfacial properties is very important for applying polymer composites to real products.

Several experimental methods are used for researching interfacial properties of polymer composites. The fragmentation test [1-9], the microbond test [10-12], the pull-out test [13-15], and the microindentation test [16-17], have all been used for interfacial analysis of composites. In this research, the fragmentation test was used and all specimens were polymeric composites, which are composed of fibers and epoxy matrix. AS4-carbon and unsized E-glass were used as fibers. A

single fiber is aligned axially in the cavity of a dog-bone shape silicone mold, and then an epoxy matrix is cured around the fiber. When tensile load is applied to the matrix, stress transfers from the matrix to the fiber through the interfacial zone between the fiber and the matrix. Since the failure strain of the embedded fibers is much lower than that of epoxy matrix, the fiber breaks before the matrix. The first break in the fiber occurs at the weakest point along the fiber length. Once the fiber is broken, the fiber stress at the point of fiber break becomes zero. As the applied force increases, more stress transfers to the fiber and thus the number of fiber breaks also increases. A fiber fragment breaks into two smaller fragments and shear stress forms near each fiber break. The fiber continues to break into smaller and smaller fragments until the fragments become too short to be broken further. The final length of the fragments is called the critical length.

Fiber fracture was observed using the fragmentation apparatus. Fiber breaks can be seen optically using photo microscopy. The crack density of fiber breaks was investigated in more detail, and the photoelastic properties were observed using polarizers. Photographs of stress birefringence were taken by a camera attached to the microscope. Debonding phenomena have been investigated as an important part in studying the fracture mechanics of polymer composites. Previous studies show that debonding occurs between the fiber and the matrix when the fiber fails during tensile loading in composites [18-20]. When the fiber breaks in single fiber composites, interfacial debonds between the fiber and the polymer matrix occur simultaneously on the observation time scale. Interfacial debonding is very important property in composites, because composites are composed of different materials and bonding at the interface can govern the mechanical properties of the composite.

Even though debonding is known to initiate simultaneously with fiber breaks and regarded as an important property in composites, the specific methods to determine the debonding length optically in a composite specimen are not presented clearly or consistently in prior work. The fragmentation test is sometimes accompanied by laser Raman spectroscopy in order to measure the stress distribution in the fiber and observe interfacial debonding [16-17, 21-22]. The experiments here, however, were done without using Raman spectroscopy. Using only microscopy with crossed polarizers, most characteristics of fiber fracture and debonding were obtained. The fiber break gap and the debonding zone are explained and defined in pictures obtained from experiments on single fiber specimens.

EXPERIMENTS

The fragmentation test has been widely used for observing various phenomena occurring at the interface between a fiber and a matrix. The advantage of this test is that the specimen preparation and testing procedures are relatively simple and much information can be obtained about damage processes. A single fiber is embedded in a matrix, and an external stress is applied to the matrix. The externally applied stress is transferred into the fiber through interfacial shear stress. As the tensile load increases, the tensile strain in the fiber also increases. Eventually, the fiber load will exceed the failure strain of the fiber and the fiber will fracture. As the load is further increased, the fiber continues to fracture into shorter fragments until the fragments are too short to break. This shortest fragment is called the critical length fiber fragment. The state where the fiber no longer fractures is defined as the saturation state. The fragmentation process can be observed through a transparent matrix using an optical microscope. The fiber fragments in a single fiber usually show a wide variation in size.

When photoelasticity is added to the optical microscopy by using crossed polarizers, the distribution of stresses can be observed around the fiber breaks. Such photoelastic analyses are a

good way to study the stress fields around a single fiber embedded in a birefringent matrix. The fragmentation tests here investigated fiber breaks against strain, initial debonding at each break, debonding growth, matrix cracks, and photoelasticity, etc. The experimental work has been done using E-glass and AS4-carbon fiber composites. Those fibers were embedded as single fibers in each specimen. The single fiber composites are particularly convenient for observing fiber breaks and interfacial debonds.

Specimen Materials

The resin used in these experiments was *Shell Epon Resin 828* that includes Diglycidyl Ether of Bisphenol A (DGEBA). The epoxy group can bond chemically with other materials such as curing agents. The curing agent used here is *m*-Phenylenediamine (*m*-PDA). Epoxy resins have several reasons for being used in composites. They adhere well to many fillers, reinforcing agents, or substrates, and do not release any volatiles or water during curing. Thus, the shrinkage after curing is usually lower than with other resins. They also have resistance to chemicals and provide good electrical insulation.

The fibers used in this experiment were carbon fibers and glass fibers. Carbon fibers have relatively low density and high elastic modulus. They are used in the aerospace field because of their low weight and high strength. Their current use has been broadened to recreational sports equipment as well as to industrial or commercial products. Due to the popularity for polymer composites, AS4-carbon fibers were used here. These fibers were manufactured by Hercules, Inc. For glass fibers, there are four main types: A-glass (high alkali), E-glass (electrical grade), ECR-glass (modified E-glass to improve chemical resistance), and S-glass (high strength). Since E-glass fibers are widely used as reinforcing materials for plastics and fiberglass products, they were used in these experiments.

Specimen Fabrication

Specimen molds are necessary to make single fiber composite specimens. Molds were made from silicone rubber compound (GE Silicone RTV-551), and a dogbone shaped iron plate was used for making dogbone shaped dents in the mold. The dogbone iron plate was attached to a glass slide with double-sided tape. The glass slides were attached to the four edges of the bottom glass slide. These plates provide a wall for the iron template. If the walls were too low, silicone gel would flow over the top during curing. A heat-resistant tape barrier on the top of glass walls was needed about one inch higher to prevent overflow of silicone. Silicone was mixed with the curing agent (dibutyl tin dilaurate) according to the product instructions. The mixing ratio of the curing agent was 1 drop per 4 *grams* of silicone, and the mixing was done in a disposable plastic container. Approximately 15 *grams* of silicone was used for one mold and only one or two molds were made at a time. Thorough mixing of silicone and its curing agent is needed. The silicone was allowed to rise to the top of the tape barrier in a vacuum oven and to cycle in and out of a partial vacuum. This cycling continues until the silicone compound fell with a full vacuum and began to lie at the bottom and bubble. The vacuum was removed slowly after bubbles appeared at the bottom for a few minutes. The next step was to cure the silicone mold. Curing was done at 45-50 °C in an oven for about 20 hours. After oven cooling, the molds were removed from the template and trimmed as needed. Since the fiber guides need to be accurate and unobstructed, the mold may need to be fastened to a glass slide to keep the mold from bowing while the matrix is curing.

The matrix materials must have a sufficiently high strain-to-failure to insure that the fiber completes its fragmentation process before the matrix fails. The failure strains of cured epoxy resin (Shell Epon 828), AS4-carbon fiber, and E-glass fiber used in this research were 3.5%, 1.3%, and 2.0%, respectively. Since epoxy resin has higher failure strain than the fibers, it was used as the

polymer matrix. Epoxy resin was mixed with curing agent (m-PDA, meta-phenylene diamine) in an aluminum container. 14 *grams* of *m*-PDA was mixed for every 100 *grams* of Epon 828. This mixture was heated at 65 °C until crystals of m-PDA melt, and then it was mixed thoroughly using a wood stick. This mixture was poured cautiously using a syringe into the silicone mold, which had a fiber installed. After a few moments, the system was equilibrated and the frame was cut away from the fiber to relieve any possible prestressed fiber conditions before the matrix curing process began. In order to make a flat top for the specimen, the matrix was covered with a flat glass slide and fixed with a wood clip. Before covering with a glass slide, a 'release agent dry lubricant' was rubbed inside the glass slide to be able to remove the slide easily from the matrix after curing and be left with a flat-topped specimen.

Single fiber specimens were made using the silicone mold. A mold was secured on a glass slide. Several molds can be prepared simultaneously on a wide glass plate. For these experiments, a single carbon fiber or a glass fiber was used. A single fiber was embedded in the center of a specimen. As shown in Figure 1 (figures at the end), a fiber was attached to an oversized (longer than the mold length) wire frame using rubber cement. Then, the fiber was aligned on sprue slots in the specimen mold and a drop of glue was dropped on each sprue slot to fix the fiber tightly. After the fiber was fixed on the mold, liquid epoxy resin was poured into the mold cavity using a syringe. The resin was injected into the mold continuously from one end to the other end to prevent air bubbles in the specimen. Some excess resin was required to prevent shrinkage away from the sides of the mold. If the amount of resin was not enough, specimen molds would be insufficiently filled after curing and incomplete due to resin shrinkage during the specimen curing process.

Curing in this research required two methods: oven curing and room temperature curing. The oven curing was done at 75 °C for two hours and then at 125 °C for two hours. The room temperature curing was to avoid residual stress in the samples. Specimens were cured at room temperature in a dark location shielded from UV radiation. Some resin may boil or bubble out of the mold during curing, and if necessary additional resin can be added. A completed single fiber specimen is shown in Figure 2. Cured epoxy resins show different properties according to curing conditions such as mixing ratio, curing agent, temperature, time, etc. The epoxy resin has a linear elastic stress-strain curve. Table 1 shows the mechanical properties of the cured epoxy resin used in this research.

Test Apparatus

A schematic picture of the apparatus of fragmentation test is shown in Figure 3. Specimens were loaded between two grips and bound tightly with 8 bolts. Two polarizers were used for observing fracture phenomena. One was on an upper part; the other was on a lower part of the equipment. A motor translates the specimen end and gives a tensile load to the specimen. When the switch of the motor is in the 'forward' position, tensile load was applied to a specimen. In the 'reverse' position, the samples were released. The recorder shows how much load was applied. With polarizers and a camera, phenomena such as fiber breaks, interfacial debonding, matrix cracking, and the resulting photoelasticity or birefringence can be observed.

Table 1. Properties of cured epoxy resin.

Tensile Strength [MPa]	70
Tensile Modulus [MPa]	2600
Shear Modulus [MPa]	970
Poisson's Ratio	0.34
Thermal Expansion Coefficient [mm/°C]	40×10^{-6}
Elongation to Failure [%]	3.5

EXPERIMENTAL RESULTS AND DISCUSSION

Photoelastic Features

The stress state near fiber breaks and the interface between the fiber and the matrix were optically observed using crossed polarizers in the fragmentation apparatus. Such microscopic observation is very useful for studying the behavior of interfacial stress in the composites. Because the epoxy matrix is transparent, fibers in the matrix are visible through the microscope. When a tensile stress was applied to the specimen externally, the specimen was stressed under tensile loading. With continuously applied stress, the embedded fiber fractured inside the matrix. The specimen exhibited birefringence colors near the fiber breaks and the interface. Figures 4 and 5 show the photoelastic stress birefringence of carbon and glass fibers, respectively, in composites.

Photoelastic analysis is a good technique for observing fibers embedded in a matrix. Many researchers have used this technique in their analyses [3,23]. From the top picture in Figure 4, carbon fiber looks very dark in the epoxy background. No external loading was applied to the specimen in this state. When an external tensile loading was applied to the specimen, the specimen extends in the loading direction. The matrix is stressed and the fiber is also under the loading by the stress transferred from matrix to fiber. Eventually, the fiber inside the epoxy matrix begins to fracture. When the fiber fails, stress birefringence is observed near the breaks as shown in the second picture of Figure 6. This optical birefringence indicates shear stress originated from the tensile loading. The shear stress is distributed near the fiber break, or the ends of break. The birefringence usually showed symmetric features at both sides of the fiber end. As the loading increased, more stress is transferred to the fiber. The interface has a higher shear stress. Higher stress on the interface caused interfacial debonding or damage between the fiber and the matrix. When there is damage at the interface between the fiber and the matrix, the interfacial bonding becomes weak and the shear strength decreases. As a result, stress birefringence became longer and flatter for higher strain. In Figure 4, the bottom picture shows a carbon fiber at the highest stress and its birefringence was very flat and long.

Glass fibers are transparent and two times thicker than carbon fibers (AS4-carbon diameter = 7.0μm, E-glass diameter = 14.0μm). Figure 5 shows a series of fiber breaks according to applied strain. Similar to the carbon fiber, the stress birefringence of a glass fiber showed a longer and flatter pattern as the strain was increased. Also, stress birefringence looked symmetric around the fiber breaks. The gap between the fiber fragments was more apparent than with a carbon fiber, because glass fiber is much brighter than its break gap. This point helped to observe the break gap. For carbon fibers, it is difficult to distinguish the break gap from the fiber because of its dark color. As the applied strain becomes higher with glass fibers, the size of the gap clearly increases. Birefringence does not show up at the fiber break, because there is no shear stress at the break.

Fiber Breaks

When a tensile load is applied to a single fiber specimen in the fragmentation test, stress is transferred from the matrix to the fiber. The fiber begins to break at some stress and continues to break as the stress increases. The fiber breaks can easily be observed using a polarized light. Figure 6 shows fiber breaks for carbon and glass fibers during tensile loading in the fragmentation test. As the carbon fibers are black, the border of fiber break in the fibers was not clearly recognized. Because the glass fibers have a bright color, the break was seen easily.

As the applied stress increases, the number of fiber breaks, *i.e.*, crack density, also increased. In other words, the fiber fragments became smaller and smaller as the applied stress got higher. At some strain, the crack density became constant and the fragment lengths stopped changing. This minimum length of fragments is called the critical length. When the critical length was obtained,

the crack density of the fiber break becomes saturated. Figure 7 shows the schematic fiber breaks from a single fiber specimen during a fragmentation test. The first break occurs at the weakest point of the fiber, but many specimens had the first break near the center of the fiber length. The subsequent breaks occurred at less weak positions. Figure 8 shows typical distributions of fiber breaks from single fiber composites during a tensile test.

The fiber break density was determined as the number of fiber breaks per millimeter of fiber length. The number of fiber breaks depended on the time when the crack numbers were counted at constant strain. For AS4 carbon fiber, the crack density of fiber breaks was usually saturated in five minutes. Thus, the cracks were counted after waiting five minutes at each strain. Then the tensile loading was applied to the specimen again until the specimen was at a new higher strain. Counting fiber breaks was done again five minutes after reaching the new strain. For E-glass fiber composites, the saturation time for fiber breaks at each strain was about 20 minutes. The break density for E-glass specimens, therefore, was measured after waiting for 20 minutes at each strain. Moon and McDonough [24] revealed that this phenomenon was due to the viscoelastic nature of the polymeric matrix, and, thus, the time dependence should be considered in order to count the number of fiber breaks accurately under a specific strain.

As the load became higher, the fiber continued to break until the number of fiber breaks saturated. Once at saturation, no new fiber breaks occurred even if the tensile load is applied continuously. Figure 9 compares the crack density of AS4-carbon and E-glass fiber specimens in the single fiber fragmentation test. The initial fiber breaks of AS4-carbon fiber occurred at the strain of 1.0~1.5%. After 1.5% strain, the density increased rapidly. When the strain reached 2.7%, the crack density showed a plateau or saturation. The critical length of the fiber fragment is obtained from this plateau region. For E-glass fibers, as expected, the crack density plot looked similar, but it was shifted to higher strains. The cracks were created around 2.0% strain and the plateau was obtained after about 3.2% strain. Strain to break AS4-carbon fiber was lower than that for E-glass fiber. There is about 1.0% strain difference for fiber break between AS4-carbon and E-glass specimens. The plateau of crack density for E-glass fiber was lower than that for AS4-carbon fiber (AS4 ~ 3.3/*mm*, E-glass ~ 2.7/*mm*).

An empirical fit model to crack density was determined using

$$f(x) = \frac{A}{1 + EXP[B(x - C)]} + D \tag{1}$$

This equation can be obtained by combining the *error function* (or, *probability integral*) and the *Avrami equation*. The best values for the parameters, A, B, C, and D were determined by the *Levenberg-Marquart* method [25]. The values of fitting parameters for this model are shown on Table 2. The values of *COD* and *STD* are also reported to give an indication of the goodness-of-fit.

Fiber Break Gap

The fiber fails earlier than the matrix during tensile loading because it has lower strain to break. Once the fiber fractures in the epoxy matrix, the fiber ends may slip leaving empty space at the position of fiber break. A simple experiment was done to see how break gaps appear under the microscope. First, a hole was made by a drill tip in an epoxy matrix (Figure 10 (a)). The empty hole was observed to be very dark through a microscope. Second, some part of a fiber was pulled out of the matrix (Figure 10 (b) & (c)). Glass fiber composites were used for this experiment, because glass fibers look bright and can be observed well in the dark space. The specimen was broken deliberately and then some parts of glass fibers were drawn from the matrix. The wide

Table 2. Values of fitting parameters for the crack density model

Fibers	*A*	*B*	*C*	*D*	*COD**	*STD***
AS4-Carbon	-3.2968	0.1886	50.5947	3.2641	0.8761	0.0441
E-Glass	-2.4527	0.2742	68.6883	2.5561	0.8925	0.0325

* Coefficient of Determination
**Standard Deviation

bright background is the epoxy matrix. The empty space looks dark. The glass fiber lies horizontally. The empty space where the fiber was removed looks much darker compared to the epoxy matrix. The border between the glass fiber and the empty space was clearly defined.

It can be concluded that empty spaces, holes, and air bubbles inside an epoxy matrix look dark. When a fiber breaks inside a matrix, broken halves of the fiber may move leaving behind some empty space near the fiber break. This space is referred to here as the fiber break gap and the break gap is created at the position of fiber break. This gap emerges simultaneously with the fiber break and it became wider as the applied strain increased. Therefore, the break gap due to the fiber failure looked black and it could easily be observed.

For single fiber specimens, typical break gaps are shown in Figure 11. Figure 11 (a) shows a schematic break gap; at low strains, the fiber will make a small gap, but the gap widens at higher strains. Glass fiber showed obvious gaps at the center of fiber breaks (See Figure 11 (b)). As commented above, the gaps looked black for glass fiber specimens. For carbon fibers, however, the break gap is not distinguished from the fiber because the opaque carbon is also black. The gap for carbon fibers can only be detected using the stress birefringence. As discussed at the previous chapter, birefringence did not appear at the fiber break because there is no shear stress there. Thus, the break gap can also be observed at the carbon fiber specimen (Figure 11 (c)) from the region of no birefringence.

When a fiber fractures in the fragmentation test, debonding between the fiber and the matrix usually occurs simultaneously. Thus, observation of fiber fracture is a tool for understanding interfacial debonding process. The behavior of the fibers is mainly dependent on the mechanical properties of fibers, curing conditions of specimens, and the interfacial bonding status. Fiber breaks can be seen easily using a polarized microscopy. By observing photoelastic birefringence of fiber fragments, specific outlines of breaks are better seen for bright fibers because fiber breaks look black. Fiber fragments vary in size. The length of the fragments has been an important function for calculating interfacial shear stress.

Shapes of photoelastic birefringence for carbon and glass fibers seen in Figures 4 and 5 show infinitesimal shear stress at the ends of fiber fragments. Theoretically, shear stress of fiber should be highest near the end of fragment. As mentioned above, however, fiber breaks accompany interfacial debonding between the fiber and the matrix near fiber ends. Therefore, shear stress decreases in debond zones. If there were no debonding near the fiber ends, photoelastic birefringence would appear differently. Figure 12 compares the expected birefringence patterns for fiber breaks without debonding and with debonding. As expected, however, all specimens in this experiment show the birefringence of fiber breaks with debonding.

Debond Zone

For fiber-reinforced composites, one of most important concerns is to observe interfacial debonding phenomena between fibers and polymeric matrices. During tensile tests, a fiber embedded in a polymer matrix takes the stress transferred from the matrix. The fiber fractures at some stress value and that fiber break causes simultaneous debonding between the fiber and the matrix. The fiber bonds with the polymer matrix, here epoxy resin, on a molecular level when the

specimen is fabricated. In other words, they connect firmly to each other when they are cured in a high temperature oven and at room temperature. In order to explain their bonding, a schematic two-dimensional picture is presented in Figure 13 (a). A fiber is embedded horizontally at the center of matrix and the dimension of matrix is reduced to enlarge the fiber size. Between the fiber and the matrix, there is the interfacial zone which surrounds the fiber inside the matrix. The interfacial zone is expressed as many bonding lines. Of course, the external loading is not applied yet and the bonding lines are in a state of equilibrium. The degree of interfacial bonding will be affected by the curing condition.

As the loading begins, the molecular bonding lines become tense (Figure 13 (b)). With further loading, the fiber fractures and then some lines near the fiber break are disconnected almost simultaneously. The fiber breaks into two fragments leaving empty gap at the point of break. Even though most bonding lines right near the fiber break are broken, the lines a little away from the break are not broken but show a tense state. The bonding lines further away from the fiber break, however, are almost not affected by the applied stress; they lie as loosely as the original regular condition, or approach the equilibrium state. Here, the debond zone is defined as the region where the molecular bonding lines are broken including the fiber break gap. The debonding zone is usually symmetric on both sides of the fiber break site. It is small for strong interfacial bonding but can be large for the weak interfacial bonds.

Debond zones can be observed using the photoelastic birefringence. As discussed in the previous chapter, birefringence formed as the specimen was loaded under tensile stress. Even though much data from interfacial debonds of composites have been presented, the definition of debonding size in real microscopic pictures has been equivocal. In this research, to explain debond zones more clearly, schematic figures were used. Figure 14 shows the features of a debond zone for E-glass fibers. Since glass fibers look bright through a microscope, it is easier to observe the debonding zone than with black carbon fibers. When the loading is applied to the single fiber specimen and then the fiber is broken, a break gap and interfacial debonding occurred. Simultaneously, photoelastic birefringence formed near the stressed fiber ends (Figure 14 (a)). The birefringence indicated that the fiber is under shear stress due to the externally applied loading. The birefringence had two different colors; there is a distinctive flat color zone at the interface between fiber and matrix near the fiber break gap. When the external loading was removed, the big birefringence disappeared but the inner flat color band is still distinctive (Figure 14 (b)). It was assumed that the interface was damaged by the fiber break, or the external loading. Therefore, the length of debond zone was determined as equal to the length of this flat color zone at the interface. The length of debond zone decreased when the external loading was released and the matrix of a specimen returns to the original position. Also, the break gap reduces itself.

This debonding process is illustrated in real pictures in Figure 15. A glass fiber fractures under the applied tensile loading, causing an obvious fiber break at the center of the fiber and the debond region symmetrically at both sides of fiber break (Figure 15 (a)). The flat band at the interface is denoted as the ‘debond zone.’ When the load was removed from the specimen, the fiber came back close to the initial position (Figure 15 (b)). With controlling angles of polarizers of the microscope, three different birefringences could be observed. As expected, the break gap size and the debond length were different from those of stress-loaded situation of (a) despite being for the same fiber break. This difference was because the fiber contracts when the loading is removed. Some part of the interface between fiber and matrix was damaged and/or there may be some slip at the interface (Figure 15 (b)). The debonding data were drawn from the loaded situation as in Figure 15 (a) because real materials are under the load and the energy should be calculated

under the loading situation. Figure 16 shows similar figures to Figure 15. Two fiber breaks are located close together. Fiber breaks and debonding zones are obviously seen under both loaded and unloaded states.

For carbon fiber composites, it was difficult to recognize the debonding zone through the microscope during tensile tests. Because carbon fiber is black, the debonding region was hardly visible. That is, the debonding flat color was not seen clearly. Some researchers have abandoned optical methods for carbon fibers. Others used Raman Spectroscopy to observe carbon fiber debonds [26-28]. If the polarizers are properly controlled, however, debond regions can be investigated by photoelastic birefringence obtained from a microscope without using Raman spectroscopy. Figure 17 has a schematic figure of the debond zone for carbon fiber specimens. When a specimen is under tensile loading, birefringence is formed at the interface between the fiber and the matrix around the fiber break. The fiber break gap is not distinctive, because the break gap looks black like the fiber itself. The gap, however, can be deduced from the stress birefringence. Since there is no stress at the fiber break gap, stress birefringence does not appear. Thus, the break gap of carbon fiber specimens can be measured from the zone with no stress birefringence near the fiber break.

With the proper use of polarizers in a microscope, a red color zone can be seen inside the big round birefringence for carbon fiber composites (Figure 17 (a)). When the loading was released, the stress birefringence disappeared, but some parts of the interface still looked different from a normal interface (Figure 17 (b)). It seems that molecular bonding between the fiber and the matrix was disconnected and slip occurred at the interface. Therefore, the distance between the two red spots in Figure 18 (a) was considered as the length of the debond zone for carbon fibers. More realistic evidence is shown in Figure 18. The specimen is under tensile loading in (a), and the loading is released in (b). When the loading was released, the debonding region could be observed more obviously with the help of polarizers.

Debond zones became longer as the externally applied loading increased. This effect is debond growth. Debond growth for E-glass and AS4-carbon fibers are shown in Figures 19 and 20, respectively. There are some special cases for debonds of single fiber composites (Figure 21). In Figure 21 (a), two breaks in the carbon fiber are so close that the debond zones at each fiber break become connected. The usual critical length for fibers is about 100 μm, but, for this specimen, the fragment length was about 50 μm. This case was very unusual, but it can occur in pre-damaged fiber specimens or mistreated specimens. Figure 21 (b) contains a large break gap with a glass fiber and a very long debonded interface. This phenomenon usually occurred for loosely bonded or very weak interfaces. When the interface is very loose, there was no fiber break in some specimens until the overall interface was debonded (Figure 21 (c)). The interface of this carbon fiber did not experience debonding until the specimen fractured. This case was also unusual and was not used as data for analyzing fiber breaks and interfacial properties.

Instantaneous (New) Debonds

When a fiber breaks into two fragments, debonding between the fiber and the matrix occurs simultaneously. Thus, debond zones are created at each fiber break. To measure the lengths of debond zones in a specimen, all debond zones for each strain were considered. For example, if 30 fiber breaks were observed at some applied strain in a specimen, 30 debond zones exist in the specimen. To get the length of debond zones at the strain, 30 lengths of debond zones were measured and then an average value of 30 lengths was taken. This average value is an experimental debonding length for that strain. This procedure was done for each applied strain, and average

values of debonding lengths were taken as experimental debonding data and plotted for corresponding strains.

To collect experimental debonding data, 10 and 11 specimens were tested for AS4-carbon and E-glass fiber composites, respectively. Debonding data were classified into two parts: instantaneous debonds and whole debonds. The following sections explain these two types debonding results in detail.

Since debondings are created at every fiber break, new debond zones are initiated whenever new fiber breaks occur. Figure 22 shows schematic features of new debonding in a single fiber specimen. Two fiber breaks occur at 2.0% strain and, at the same time, two new debondings (① and ②) are created. At 3.0% strain, another two new fiber breaks are initiated accompanied by two new debonding zones (③ and ④). Similarly, new debondings (⑤ and ⑥) are created at 4.0% strain. These new debondings are called *instantaneous* debonds. These debonds are only the new zones found when a new fiber break occurs. For example, in Figure 22, debondings ① and ② at 2.0% strain are instantaneous debonds, but, at 3.0% strain, ① and ② are no longer instantaneous. Only ③ and ④ are instantaneous debonds at 3.0% strain. At 4.0% strain, ⑤ and ⑥ are instantaneous debonds, but ①, ②, ③, and ④ are not instantaneous debonds. Therefore, only new debondings at a strain were considered for collecting instantaneous debonding data.

Lengths of debonding zones were measured as debonding data. An average value of lengths of all instantaneous debond zones at a strain was taken as experimental results for new debond growth. For example, at 2.0% strain in Figure 22, the length of instantaneous debond zones is an average value of new debondings ① and ②. For 3.0% strain, only new debondings ③ and ④ are used for taking an average value of instantaneous debond zones. At 4.0% strain, an instantaneous debond length is an average value of new debondings ⑤ and ⑥, and debondings ①, ②, ③ and, ④ are excluded.

Figures 23 and 24 show instantaneous debond lengths for AS4-carbon and E-glass fiber composites, respectively. Debond lengths are expressed as 'debond growth'. It is obtained from average new debond length divided by fiber diameter. For example, the maximum value of debond growth for AS4-carbon fiber specimen was about 10 *fib. dia.* (fiber diameter) in Figure 23. This value corresponds to 70 μm, which is 10 times 7.0 μm. For E-glass fiber (Figure 24), a maximum value was about 14 *fib*. *dia*. It is calculated as 196 μm (= 14 x 14.0 μm).

When strain increased, new fiber failures and new instantaneous debonding occurred. These new instantaneous debond zones that occurred at higher strain are larger than the debond zones that occurred at lower strain. In other words, the length of the instantaneous debond zone becomes longer as the strain increases. Instantaneous debond zones, however, show a maximum length at some strain, and then decreased as the strain increased further. The decrease was caused by less energy being reduced by fiber breaks as the fiber fragments got shorter.

Whole Debonds

Whole debonds mean the average of all debonds present at any strain. That is, whole debonds included both instantaneous debonds and pre-existing debonds which were created in previous strain stages. For example, at 2.0% strain in Figure 24, whole debonds means debonding ① and ②. At 3.0% strain, whole debonds includes new debondings ③ and ④ as well as pre-existing debondings ① and ②. Whole debonds at 4.0% strain includes all debondings ①, ②, ③, ④, ⑤, and ⑥. An average value of whole debonding lengths is taken from all six debondings.

When strain stays constant, the lengths of debond zones hardly increases. As the applied strain increases, debond zones may get longer. That is, debond lengths increase as strain goes up. Experimental data of whole debond lengths for AS4-carbon and E-glass fiber specimens are

plotted in Figures 23 and 24, respectively. Whole debond lengths were plotted as 'debond growth' in fiber diameters as done for instantaneous debond lengths. The largest debonding length observed in AS4-carbon fiber was about 119 μm (17 *fib*. *dia*. times 7.0 μm) at 2.7% strain. For E-glass fiber, the largest length observed was about 224 μm (16 *fib*. *dia*. times 14.0 μm) at 3.3% strain. As described before, instantaneous debond lengths increased at low strains and then decreased at higher strains. Whole debond lengths, however, did not show any decrease at higher strains. They increased continuously until the specimen failed.

To compare instantaneous debonds and whole debonds, both debond lengths are plotted in one figure for AS4-carbon and E-glass fiber specimens. For AS4-carbon, instantaneous debond lengths showed a maximum value near 2.3% strain, but whole debond lengths continued to increase (See Figure 23). The difference between these two results represents the extent of debond propagation of the existing debonds at each strain level. As described before, whole debonds include instantaneous debonds. Even if there were some drops in instantaneous debond lengths at higher strains, total (whole) debond lengths increased at the same strains.

E-glass fiber specimens showed a similar trend (See Figure 24). Instantaneous debond lengths increased until 3.0% applied strain, but whole debond lengths continued to increase without any decrease of lengths. Again, the curves differ when debond propagation becomes significant between observations of debond sizes.

Investigation of fiber break gaps is a good tool for observing defects in composite materials. Also, fiber break gaps are included to measure the lengths of debond zones. Some empty spaces including fiber break gaps inside epoxy matrix look relatively dark. Thus, those defects can be observed clearly in a transparent epoxy matrix. A fiber break gap is observed more clearly in glass fibers than in carbon fibers, because glass fibers look bright while break gaps look dark. For carbon fibers, they are black and thus it is difficult to distinguish dark break gaps from carbon fibers.

Interfacial properties play a critical role in composite materials. To investigate the properties, this research dealt with interfacial damage or debonding between the fiber and the matrix. First, debond zones near fiber breaks were observed using two polarizers. By controlling the angle of the polarizers, shear stresses near breaks can be visible using microscopy. These stresses appear as photoelastic birefringence. The unidirectional lengths of debond zones were determined from the photoelastic birefringence. Thus, debond lengths can be measured easily and clearly in the fragmentation test. Debond lengths include fiber break gaps and were used for the analysis of thermoelastic fracture mechanics in this research. Debond zones were classified into instantaneous (new) debonds and whole (total) debonds. Lengths of instantaneous debonding increased and then decreased as the applied strain increased. Whole debond, however, increased continuously.

ANALYSIS OF EXPERIMENTAL RESULTS

Energy Release Rate of a Single Fiber Fragment

Many fracture models for composites have been developed using linear elastic fracture mechanics, because high modulus fiber reinforced composites often show nearly linear elastic behavior before fracture. For fracture mechanics, it is assumed that cracks propagate when the energy release rate due to crack growth exceeds the fracture toughness of the composite. The required energy release rate (G), which includes residual stresses, can be calculated from a general energy balance of

$$G = -\frac{d\Pi}{dA} = \frac{d(W-U)}{dA} \tag{2}$$

where Π is thermoelastic potential energy, W is external work including work due to residual stresses, U is thermoelastic internal energy, and dA is an increment in total crack area. The terms can be calculated using linear thermoelasticity methods. This energy balance equation is applied to analyze the materials showing linear elastic behavior such as AS4/epoxy and E-glass/epoxy composites used in this research. Even though the model composite is assumed to be linearly elastic, there are more factors that affect the energy release rate. Residual stresses, crack surface tractions, and imperfect interfaces are major factors that make fracture mechanics of composites complex. Nairn [26] solved these mechanics problems partitioning total stresses into exact initial stress and approximate perturbation stress. In the fragmentation test, he assumed that a single fiber was embedded in a large amount of matrix and the specimen was loaded in tension until the fiber fragments. Figure 25 shows a cross section of a single fiber fragment of length l and radius r_f embedded in an infinite amount of matrix. l_d is debond length and σ_0 is far-field matrix axial stress. From this model, Nairn obtained the energy release rate as

$$G = \pi r_f^2 \psi_\infty^2 \frac{d}{dA}\left\{\frac{l_d}{2E_A}\left[1-\frac{\psi_f l_d}{r_f}+\frac{\psi_f^2 l_d^2}{3r_f^2}\right]-\left(1-\frac{\psi_f l_d}{2r_f}\right)\left\langle w_f^{(p)}\left(\left(l-l_d\right)/2\right)\right\rangle\right\} \tag{3}$$

where E_A is the axial (fiber direction) modulus. ψ_∞ indicates the far-field fiber stress, and ψ_f is the friction term which can be measured as the ratio of the fricative shear stress to the far-field, axial fiber stress. $w_f^{(p)}$ is the perturbation axial displacement at the interface between the fiber and the matrix, and the $\langle\ \rangle$ brackets indicate the averaging over the cross section of the fiber. Therefore, the energy release rate depends on the average axial fiber displacement at the debond tips or on $\left\langle w_f^{(p)}\left(\left(l-l_d\right)/2\right)\right\rangle$. This term will eventually require some approximate stress analysis and evaluation of the appropriate derivative for damage growth (dA). All other assumptions are expected to be reasonable and Equation (3) can be used for the basis from fracture mechanics analysis of the fragmentation test.

Finite Fracture Mechanics

Finite fracture events of fiber fracture and debonding means that composites fail by a series of discrete fracture events rather than by continuous crack growth. The term finite fracture mechanics was first used by Hashin [29] to describe the subject of predicting fracture events. Finite fracture mechanics assumes that the fracture event occurs when the total energy released by that fracture event exceeds the critical energy release rate or toughness of the material for that failure mechanism. As observed experimentally on fragmentation specimens, fiber breaks are usually accompanied by a certain amount of interfacial debonding between the fiber and the matrix. A fiber break with debonding can be a fundamental case of fracture event in the fragmentation test. A finite fracture mechanics analysis of fiber break and simultaneous debonding assumes fiber fails at some fiber strength and then uses energy balance to calculate extent of debonding damage.

The fiber fracture in a single fiber fragmentation test is accompanied by instantaneous interfacial debonding between the fiber and the matrix near the fiber break site. The total energy released on going from an undamaged fiber to damaged fiber fragment is follows.[26]

$$\Delta G dA = \pi r_f^2 \psi_\infty^2 \left\{\frac{l_d}{E_A}\left[1-\frac{\psi_f l_d}{r_f}+\frac{\psi_f^2 l_d^2}{3r_f^2}\right]-\left(1-\frac{\psi_f l_d}{2r_f}\right)\left\langle w_f^{(p)}\left(l_d/2, l/2, l_d, l_d\right)\right\rangle\right.$$

$$-\left(1-\frac{\psi_f l_d}{2r_f}\right)\left\langle w_f^{(p)}\left((l-l_d)/2,l/2,l_d,l_d\right)\right\rangle+\left(1-\frac{\psi_f l_d}{2r_f}\right)\left\langle w_f^{(p)}\left((l-l_d)/2,l,l_d,l_d\right)\right\rangle\Bigg\} \quad (4)$$

where $\left\langle w_f^{(p)}\left(l_d,l,l_d,l_d\right)\right\rangle$ is the average axial fiber displacement at one side debond tip for a fiber fragment of length l with debond size l_d. The model predicting the amount of instantaneous debonding was obtained by equating the total energy released (ΔGdA) to the total energy required ($\pi r_f^2\Gamma_f+2\pi r_f l_d\Gamma_d$ where Γ_f is the fiber fracture toughness and Γ_d is the debonding fracture toughness). Therefore, the interfacial debonding fracture toughness, Γ_d, was calculated from the debonding data with known Γ_f as

$$\Gamma_d=\frac{r_f\psi_\infty^2}{2E_A}\Bigg\{\left[1-\frac{\psi_f l_d}{r_f}+\frac{\psi_f^2 l_d^2}{3r_f^2}\right]-\frac{E_A}{l_d}\Bigg[\left(1-\frac{\psi_f l_d}{2r_f}\right)\left\langle w_f^{(p)}\left(l_d/2,l/2,l_d,l_d\right)\right\rangle$$
$$+\left(1-\frac{\psi_f l_d}{2r_f}\right)\left\langle w_f^{(p)}\left((l-l_d)/2,l/2,l_d,l_d\right)\right\rangle-\left(1-\frac{\psi_f l_d}{2r_f}\right)\left\langle w_f^{(p)}\left((l-l_d)/2,l,l_d,l_d\right)\right\rangle\Bigg]\Bigg\}$$
$$-\frac{\Gamma_f r_f}{2l_d} \quad (5)$$

This equation was used for analyzing fragmentation experiments and predicting interfacial fracture toughness. The main experiment is to measure the interfacial debond length at a fiber break as a function of the applied strain. The interfacial debonding fracture toughness, Γ_d, can calculated at each data point using the known values of ψ_f and Γ_f. The debond length, l_d, increases with the applied strain because the fiber break and fragment are assumed to be isolated. However, when neighboring fiber breaks interact with each other, the debond length increases up to some strain value and then decreases at higher strain. For the long fragment limit, or low strain range, the total energy release rate for debond propagation becomes

$$\Delta G_d=\frac{r_f\psi_\infty^2}{4E_A}\left[\left(1-\frac{\psi_f l_d}{r_f}\right)^2-\frac{\psi_f}{\beta r_f}\left(3-\frac{2\psi_f l_d}{r_f}\right)\right] \quad (6)$$

and the toughness equation becomes more briefly as follows.

$$\Gamma_d=\frac{r_f\psi_\infty^2}{4E_A}\left[1-\frac{\psi_f l_d}{r_f}+\frac{\psi_f^2 l_d^2}{3r_f^2}+\frac{2}{l_d\beta}\left(1-\frac{\psi_f l_d}{2r_f}\right)\left(1-\frac{\psi_f l_d}{r_f}\right)\right]-\frac{\Gamma_f r_f}{2l_d} \quad (7)$$

where β is a Shear-lag parameter [30] and can be measured from the following equation.

$$\left\langle w_f^{(p)}\left(z=l_d/2,l\to\infty\right)\right\rangle=-\frac{1}{\beta E_A}\left(1-\frac{\psi_f l_d}{r_f}\right) \quad (8)$$

Analysis Results

As described earlier, instantaneous debonds mean new debonds occurring at each new fiber break as the fiber breaks into smaller fragments. As seen in Figures 23 and 24, the experimental results for new debond length increase at low strain, but, for higher strain, the fiber breaks begin

to interact and new debond lengths decrease. The analysis of instantaneous debond growth was done using the shear-lag analysis [30]. First, the strain at which the first fiber break occurred was found. Then, an initial debond size (l_d) was measured using the long fragment limit equation of Eq. (6). The strain at the first fiber break was the starting strain for the rest of the calculation. The procedure of the analysis was as follows.

a. As the strain increases, broken fiber fragments break into smaller fragments. Here, the strain required to cause the new shorter fragment length to break was found. This calculation uses the current debond size that affects the fiber stress and thus looks at the stress in the fiber. Fiber break density was determined at this stage.
b. Next, the energy release rate (ΔG_d) for debond propagation was calculated using Equation. (6) and compared to the debond toughness (Γ_d) from Equation (7). If the energy release rate exceeds the debond toughness, the debond length is allowed to grow until the energy release rate no longer exceeds the toughness. This growth requires a numerical solution of $\Delta G(l_d) = \Gamma_d$ at the current strain.
c. As the applied strain increases, the crack density of fiber breaks increases, too. Eventually, the breaks begin to interact with one another. Therefore, for higher strain, the long fragment limit model is no longer useful, but a model valid for any fragment length is needed. For any fragment lengths, the energy release rate (ΔG) for fiber break and interfacial debonding is calculated from Equation (4).
d. Using ΔG calculated in step *c* and experimental data of debonding length (l_d), Γ_d was determined for any fragment length model using Equation (5).
e. Next, new strain is obtained and repeated *a* through *d* until the maximum strain as an input parameter is reached.

The predicted lines analyzed for new debond growth for AS4-carbon and E-glass composites are shown in Figure 23 and 24, respectively. The lines include the friction effect occurred during debonding at the interface between the fiber and the matrix, and they look close to experimental results. The predicted values of interfacial debonding toughness (Γ_d) for both composites are 220 J/m^2 for carbon and 105 J/m^2 for glass.

The whole debond at some strain includes both the instantaneous (new) debonds created at the current strain and the previously existing debonds created at previous strains and perhaps subsequently propagated. While new debond lengths increase at low strain and then decreased at high strain, whole debond lengths increase continuously at all strains, as seen in Figures 23 and 24. The analysis procedure for whole debonds was similar to the new debonds analysis. The difference is which debonds were considered at each strain. The length of any debonds created in previous strain increases at next higher strain. Interfacial debonding toughness analyzed for whole debond for AS4-carbon and E-glass fiber specimens was predicted to be 130 J/m^2 and 98 J/m^2, respectively. The predicted debonding growth lines also look close to experimental data. Table 3 indicates the interfacial debonding toughness and the friction value for instantaneous and whole debond data of AS4-carbon and E-glass composites. For both fiber composites, the interfacial debonding toughness of new debonds is higher than that of whole debonds. It is considered that

Table 3. Comparison of interfacial debonding energy (Γ_d) of instantaneous (new) debond and whole debond.

Fiber	Debond Growth	Interfacial Debond Energy Γ_d [J/m^2]	Friction ψ_f
AS4-Carbon / Epoxy	New	220	0.006
	Whole	130	0.008
E-Glass / Epoxy	New	105	0.010
	Whole	98	0.004

the instantaneous debond includes all energy of event and may have contribution from kinetic energy, but the whole debond is only propagation of cracks and then could be lower.

CONCLUSIONS

In order to measure fiber breaks accurately, it is necessary to wait until saturation of fiber breaking at each strain. The saturation time was about five minutes for AS4-carbon fibers and about twenty minutes for E-glass fibers. Since the tensile stress is constant on a whole specimen, there is no special rule about where first fiber break occurs. The order of fiber breaks was very irregular, but eventually led to roughly periodic breaks. Photoelasticity is useful to investigate fiber failure and interfacial debonding in model composites. Using photoelasticity, the fiber break gap and the debonding zone between the fiber and the polymeric matrix can be clearly observed. The method deals with even carbon fibers which previously is thought to be unsuitable for such optical methods. Photoelastic birefringence of shear stress near a fiber break is highest at the ends of a fiber fragment. Since fiber breaks accompany interfacial debonding near fiber breaks, however, shear stress of interface decreases much in the debond zone. Empty space in an epoxy matrix looks dark through a microscope. Fiber break gaps of E-glass fiber were thus observed clearly. For AS4-carbon fiber, however, it was difficult to distinguish break gap from carbon fiber because of the dark color of carbon fiber. The break gap size, however, could be estimated from birefringence results.

Debond lengths were observed clearly using crossed polarizers in the fragmentation test. This new visual method provides the simpler measurement and the more precise results than using the Laser Raman Spectroscopy. Debond zones were classified into two types of debonds: instantaneous debonds and whole debonds. The experimental lengths of instantaneous debonds increased at low strain and then decreased at high strain. The strain that instantaneous debonds began to decrease was about 2.3% for AS4-carbon fiber and about 3.0% for E-glass fiber. The experimental lengths of whole debond increased continuously and then saturated at higher strain. From the experimental data of fiber breaks and interfacial debond lengths, the interfacial debonding toughness between the fiber and the matrix was analyzed for each composite system using the energy method. The predicted interfacial debond energy, Γ_d, of AS4-carbon/epoxy was 220 J/m^2 and 130 J/m^2 for instantaneous debond growth and whole debond growth, respectively. For E-glass/epoxy, Γ_d was obtained as 105 J/m^2 and 98 J/m^2 for instantaneous debond growth and whole debond growth, respectively. The results show that the interfacial toughness of new debond is bigger than that of whole debond because more energy is released in the new debond occasion.

The photoelastic results of this research give the better and more precise tool to observe the fiber fracture and interfacial debonding phenomena in single fiber composites, and, further, they can be applied usefully for studying and analyzing fracture events of multi-fiber composites.

ACKNOWLEDGEMENTS

This work was supported by a grant from the Mechanics of Materials program at National Science Foundation (CMS-9713356).

REFERENCES

1. Wadsworth, N. J. and Spilling, I. 1968. *British Journal of Applied Physics*, **1:**1049-1058.
2. Fraser, A. A., Ancker, F. H., and DiBenedetto, A. T. 1975. *Proc. 30th Conf. SPI Reinforced Plastics Division*, Section 22-A:1-13.
3. Drzal, L. J., Rich, M. J., and Lloyd, P. F. 1982. *J. Adhesion*, **16:**1-30.
4. Miller, B., Muri, P., and Rebenfeld, L. 1987. *Composites Science & Technology*, **28:**17-32.
5. Penn, L. S. and Lee, S. M. 1989. *J. Composite Technology & Research*, **11**:23-30.
6. Day, R. J. 1993. *Manchester Material Science Center*, Grosvenor St., Manchester M1 7HS.
7. Wagner, H. D., Gallis, H. E., and Wiesel, E. 1993. *J. Materials Science*, **28:**2238-2244.
8. Patrikis, A. K., Andrews, M. C., and Young, R. J. 1994. submitted to *Composites Science & Technology*.
9. Bannister, D. J., Andrews, M. C., Cervenka, A. J., and Young, R. J. 1995. *Composites Science & Technology*, **53:**411-421.
10. Fraser, W. A., Ancker, F. H., DiBenedetto, A. T., and Elbirli, B. 1983. *Polymer Composites*, **4:**238-248.
11. Bascom, W. D., Yon, K. J., Jensen, R. M., and Cordner, L. 1991. *J. Adhesion*, **34:**79-98.
12. Dibenedetto, A. T. 1991. *Composites Science & Technology*, **42:**103-123.
13. Verpoest, I., Desaeger, M., and Keunings, R. 1990. *Controlled Interphases in Composite Materials*, 653-666.
14. Feillard, P., Desermot, G., and Favre, J. P. 1994. *Composites Science & Technology*, **50:**265-279.
15. Detassis, M., Pegoretti, A., and Migliaresi, C. 1996. *J. Materials Science*, **31:**2385-2392.
16. Robinson, I. M., Zakikhani, M., Day, R. J., Young, R. J., and Galiotis, C. 1987. *J. Materials Science Letters*, **6:**1212-1214.
17. Melanitis, N., Galiotis, C., Tetlow, P. L., and Davies, C. K. L. 1993. *Composites*, **24:**459-466.
18. Wagner, H. D., Nairn, J. A., and Detassis, M. 1995. *Applied Composite Materials*, **2:**107-117.
19. Detassis, M., Frydman, E., Vrieling, D., Zhou, X. F., Nairn, J. A., and Wagner, H. D. 1996. *Composites*, **27A:**769-773.
20. Nairn, J. A. and Wagner, H. D. 1996. *Advanced Composites Letters*, **5:**131-135.
21. Huang, Y. and Young, R. 1994. *J. Composites Science & Technology*, **52:**505-517.
22. Andrews, M. C., Bannister, D. J., and Young, R. J. 1996. *J. Materials Science*, **31:**3893-3913.
23. DiLandro, L., DiBenedetto, A. T., and Groeger. 1988. *J. Polymer Compos*ites, **9:**209-221.
24. Moon, C-K. and McDonough, W.G. 1998. *Journal of Applied Polymer Science*, **67**:1701-1709.
25. Press, W. H., Flannery, B. P., Teukolsky, S. A., and Vetterling, W. T. 1986. *Numerical Recipes*, Cambridge University Press, Cambridge.
26. Nairn, J. A. 2000. *International Journal of Fracture*, **105**:243-271.
27. Chou, C. T., Gaur, U., and Miller, B. 1992. *Composite Science & Technology*.
28. Young, R. J. and Andrews, M. C. 1994. *Materials Science and Engineering*, **A184**:197-205.
29. Hashin, Z. 1996. *Journal of the Mechanics and Physics of Solids*, **44**:1129-1145.
30. Nairn, J. A. 1997. *Mechanics of Materials*, **26**:63-80.

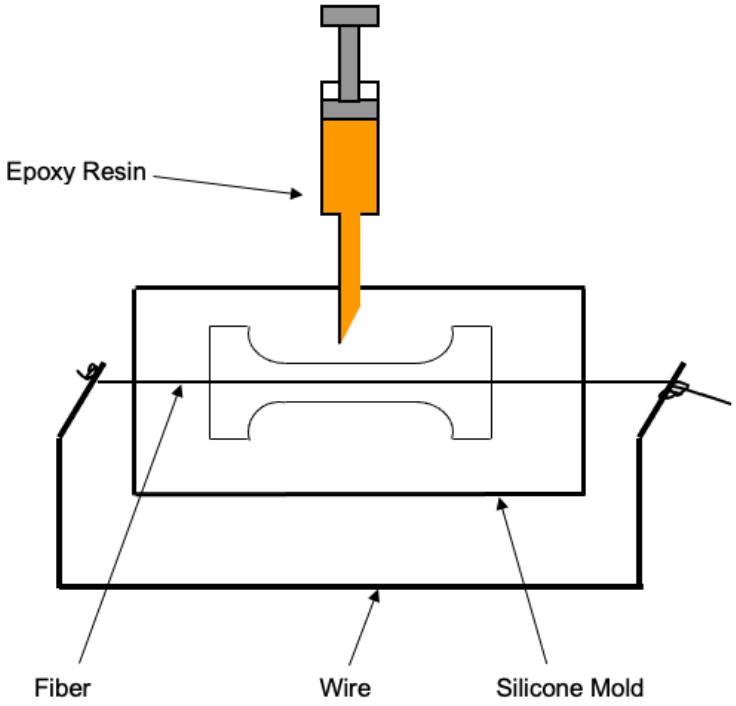

Figure 1. A single fiber is aligned over the silicone specimen mold and the liquid Epoxy is poured into the dent of the mold.

<Top-View>

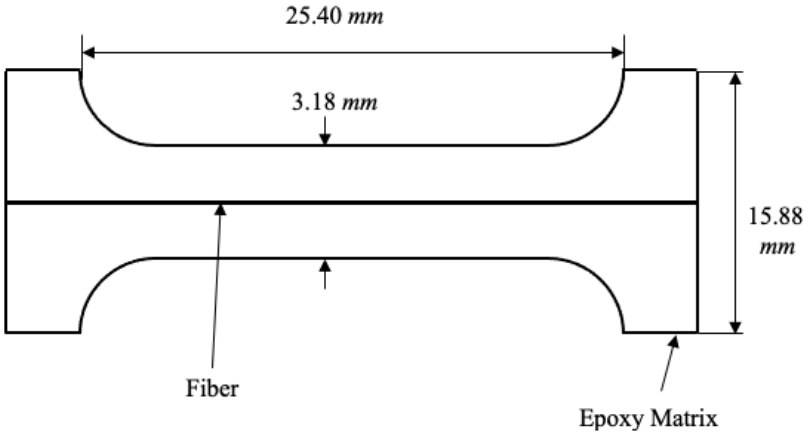

<Side-View>

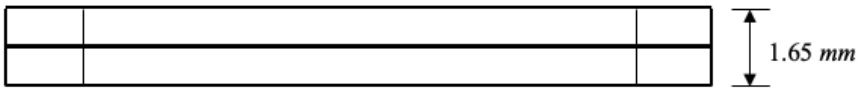

Figure 2. A single fiber composite specimen.

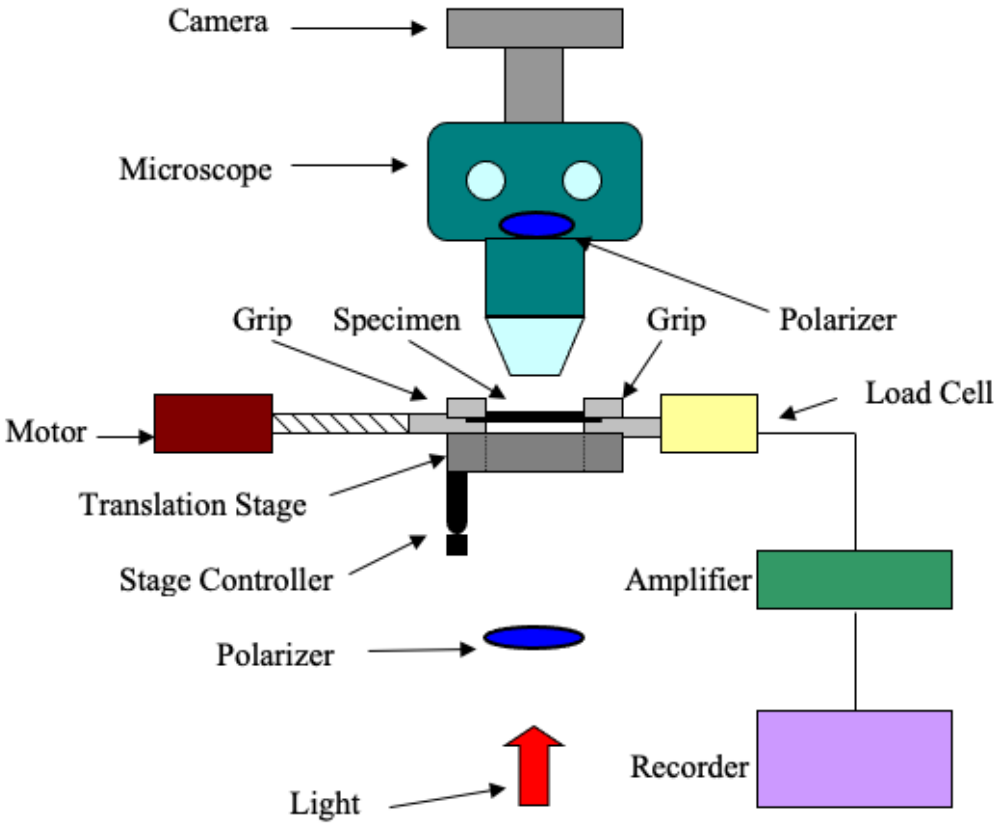

Figure 3. Schematic features of the fragmentation test apparatus.

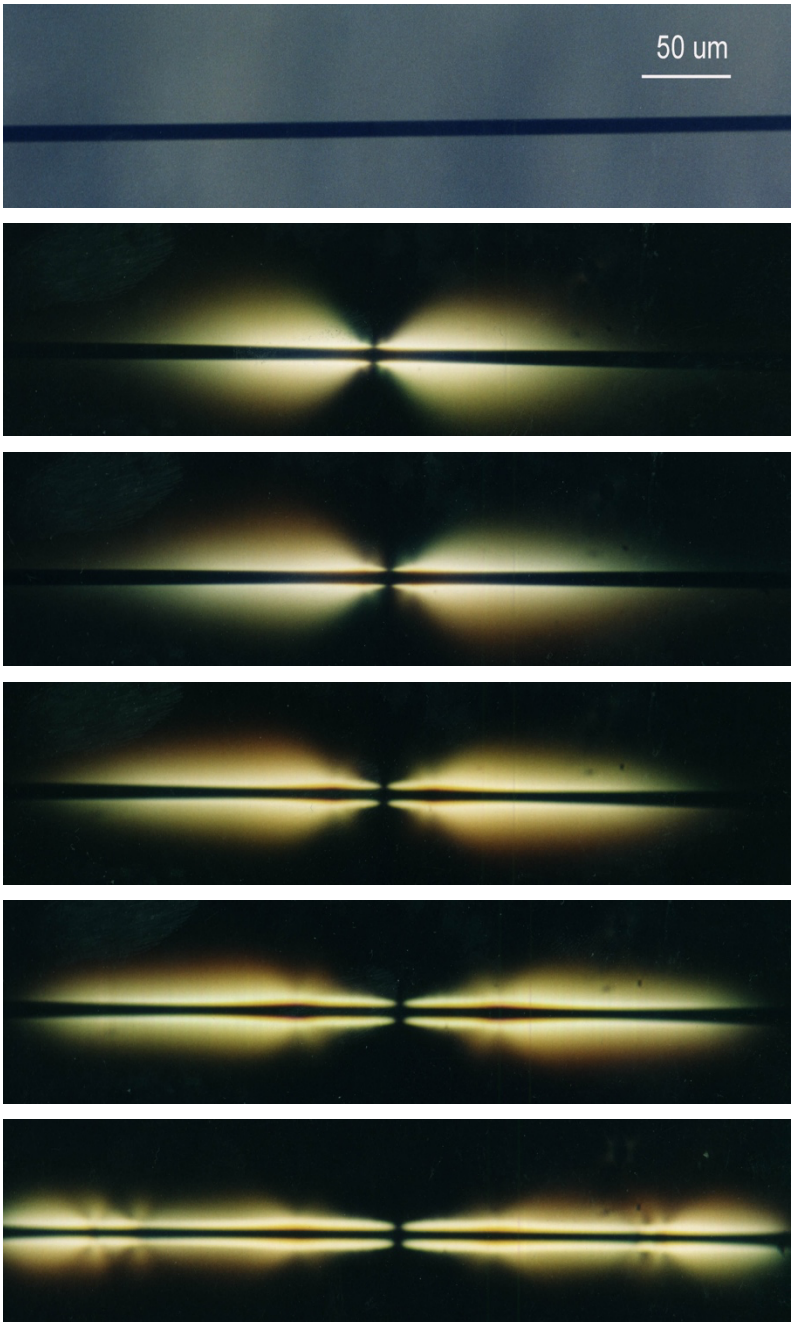

Figure 4. Photoelastic birefringence of stress around a fiber break of single carbon fiber composites.

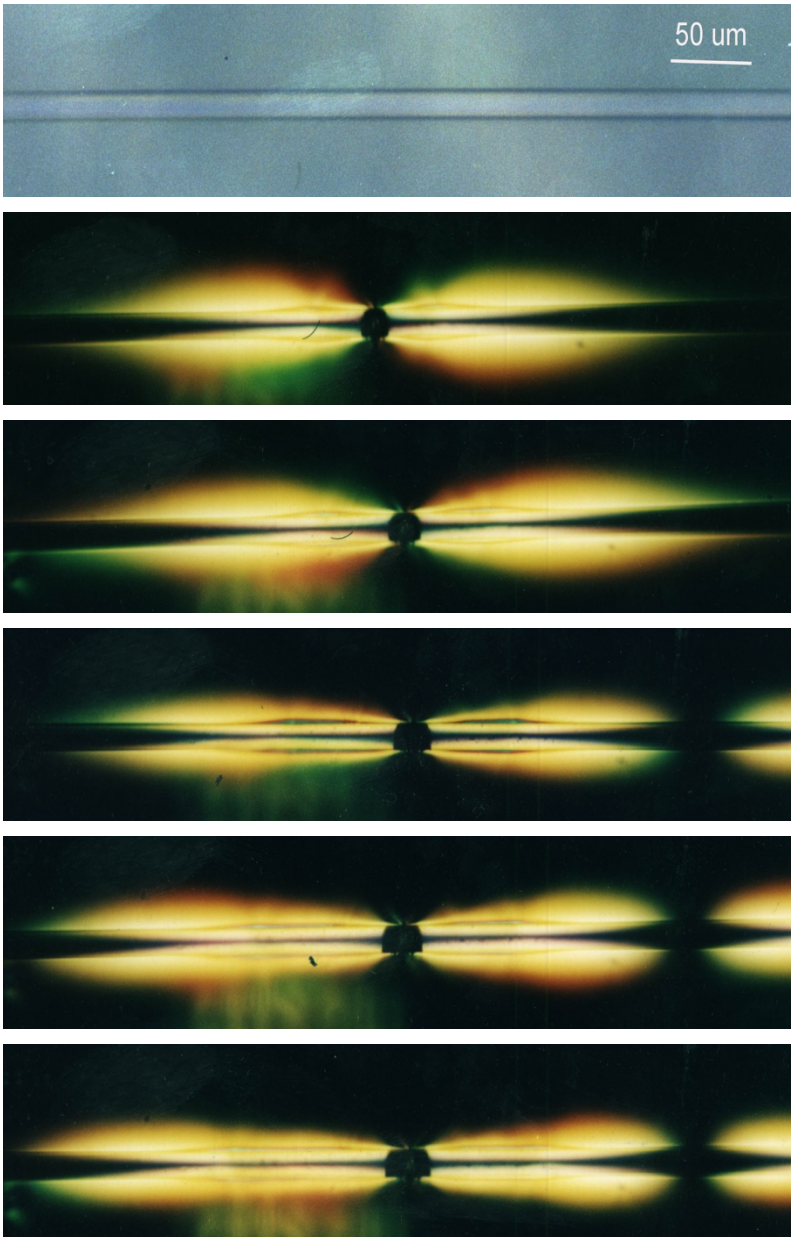

Figure 5. Photoelastic birefringence of stress around a fiber break of single glass fiber composites.

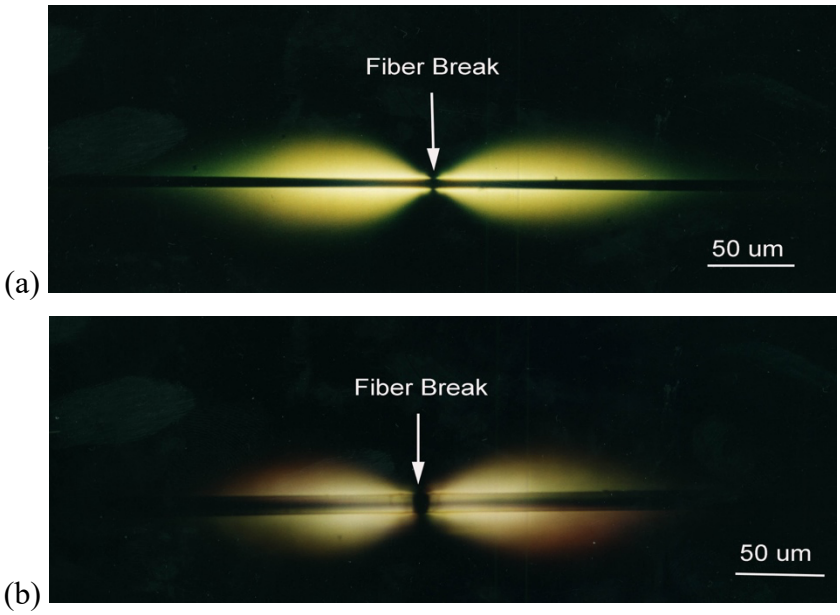

Figure 6. The fiber break of a single fiber specimen during tensile test. (a) AS4 carbon fiber, (b) E-glass fiber.

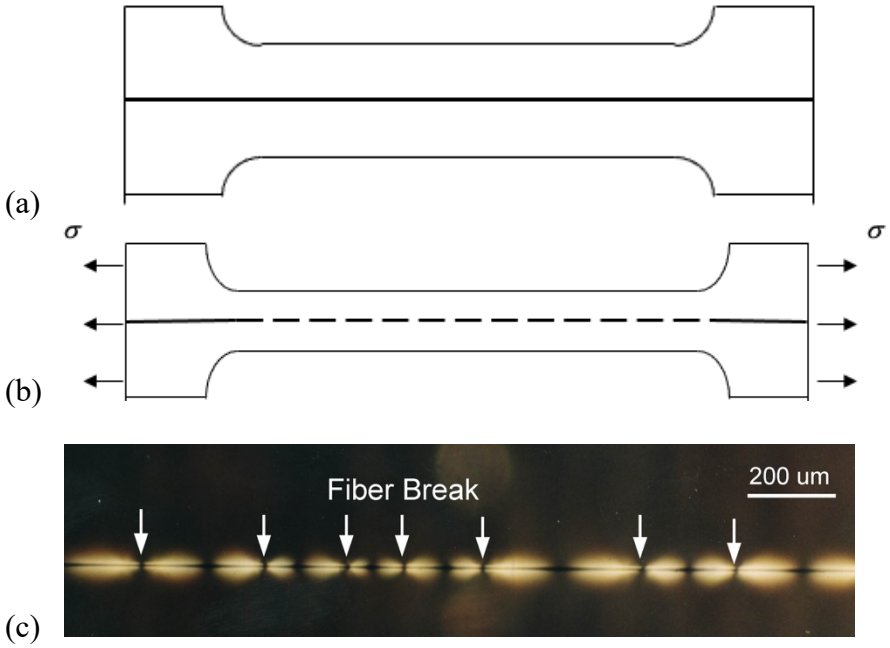

Figure 7. A single fiber specimen during the fragmentation test. (a) Before tensile loading, (b) and (c) After tensile loading.

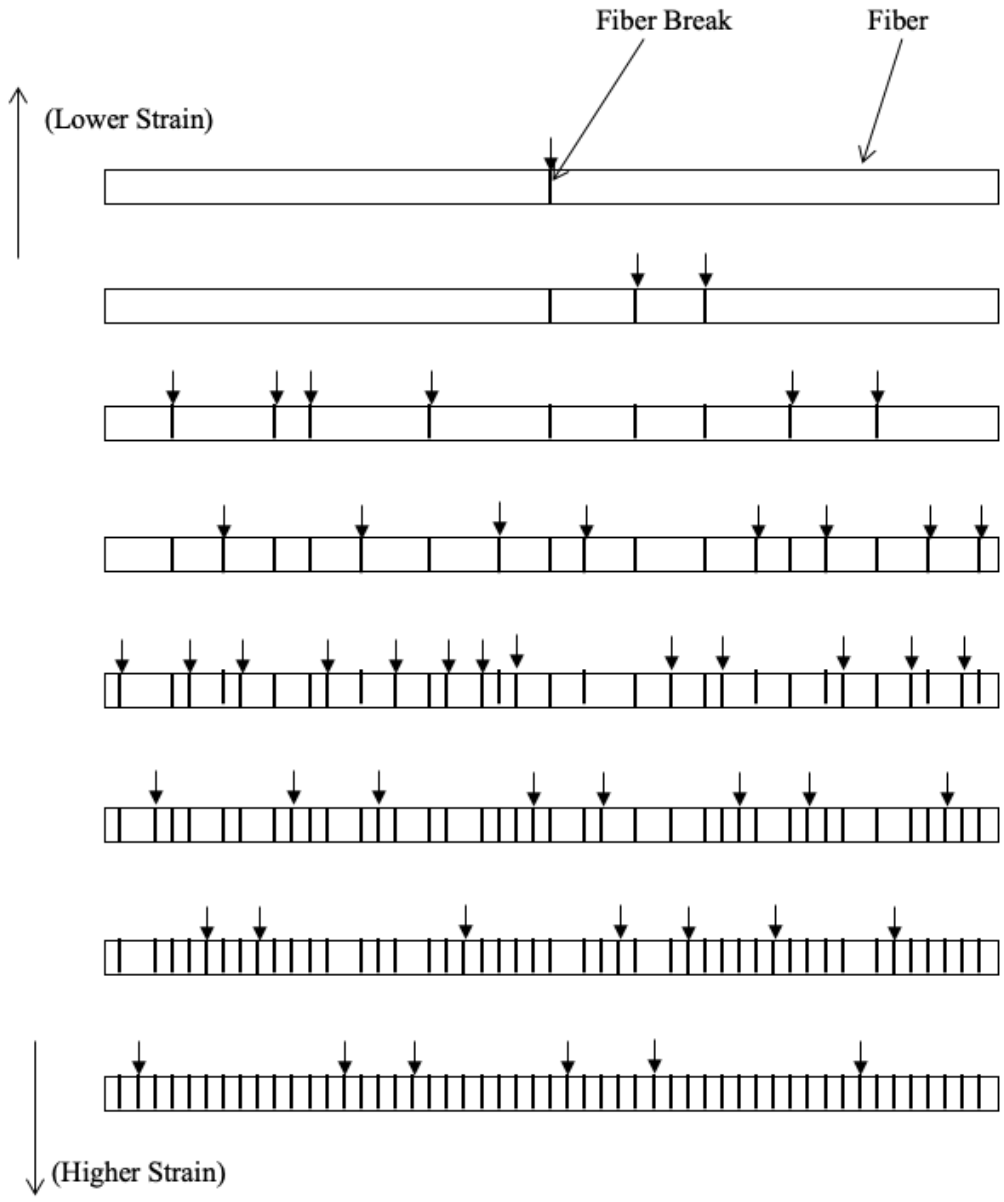

Figure 8. The distribution of fiber breaks on single fiber composites during tensile loading. The arrow (↓) means a new break created at the strain.

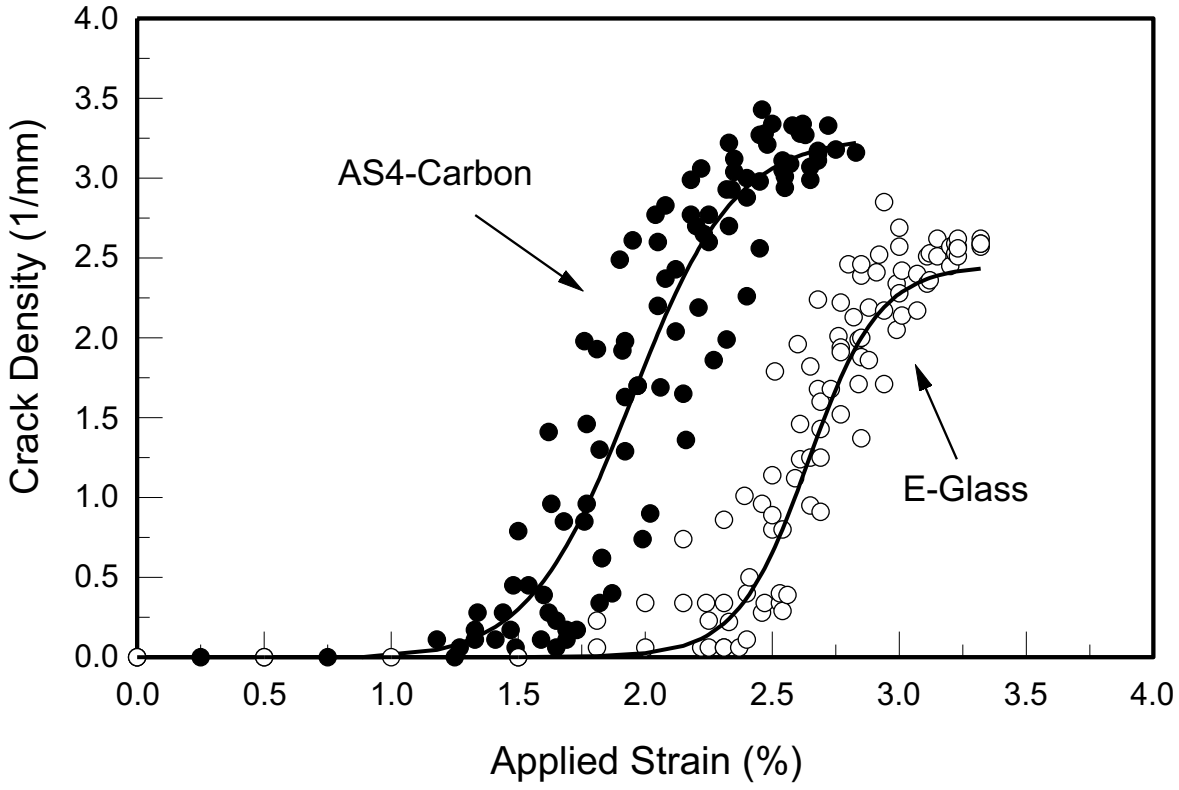

Figure 9. Crack density of AS4 carbon fiber and E-glass fiber as a function of applied strain.

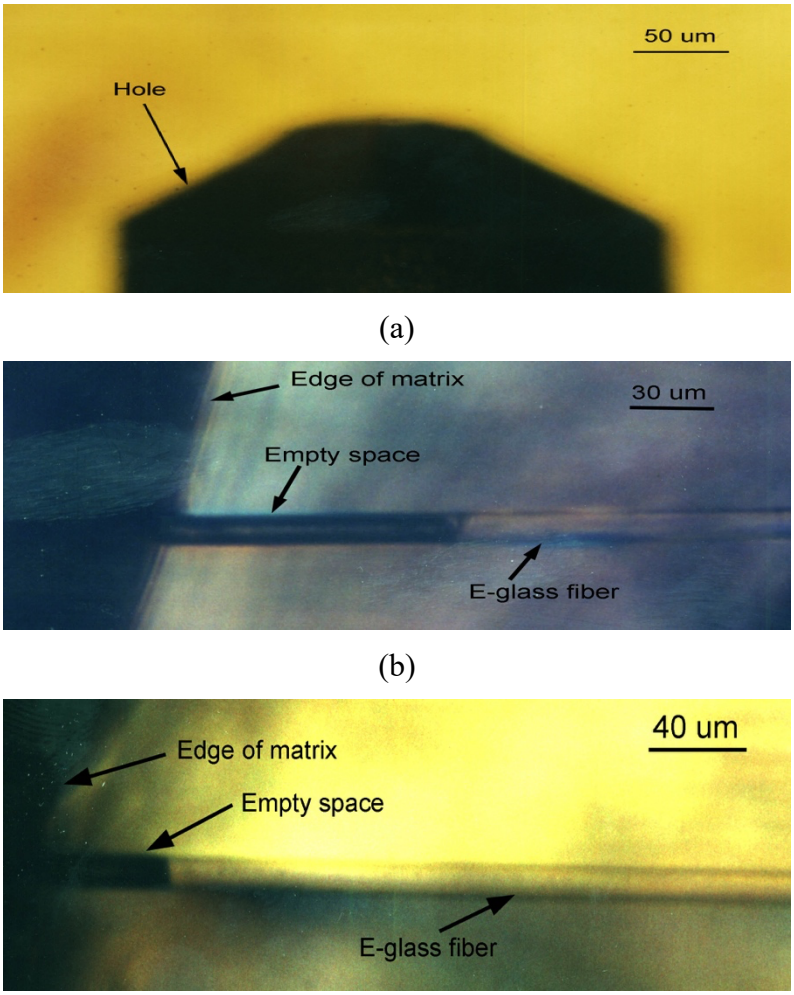

Figure 10. Examples of empty space in the epoxy matrix. (a) A hole made by drill bit, (b) and (c) Empty space made by pulling out E-glass fiber.

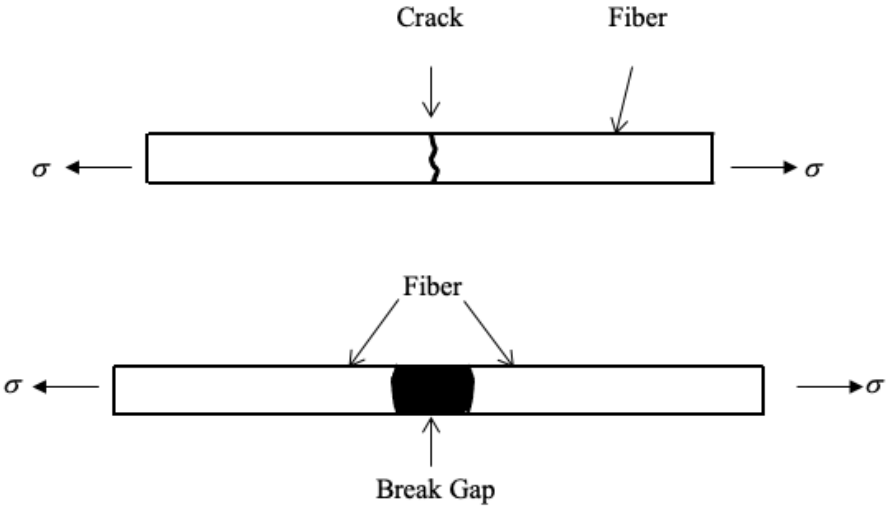

(a)

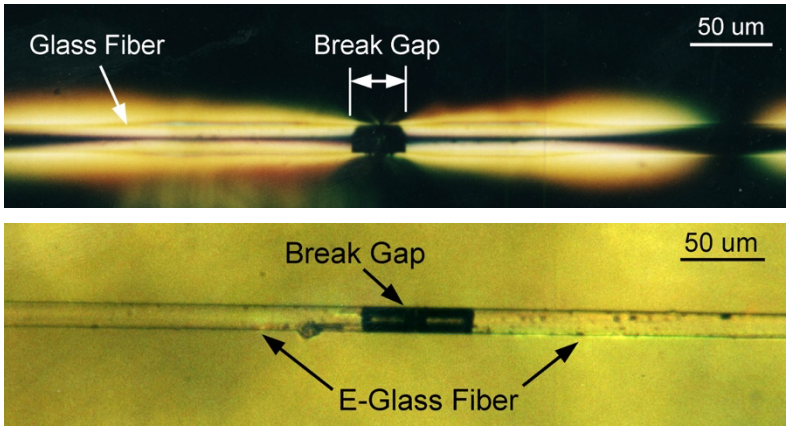

(b)

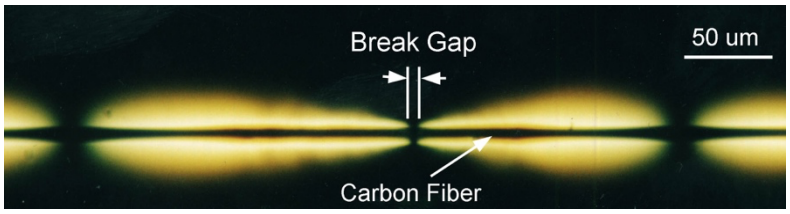

(c)

Figure 11. Examples of fiber break gap. (a) Schematic figures, (b) E-glass fiber, (c) AS4 carbon fiber.

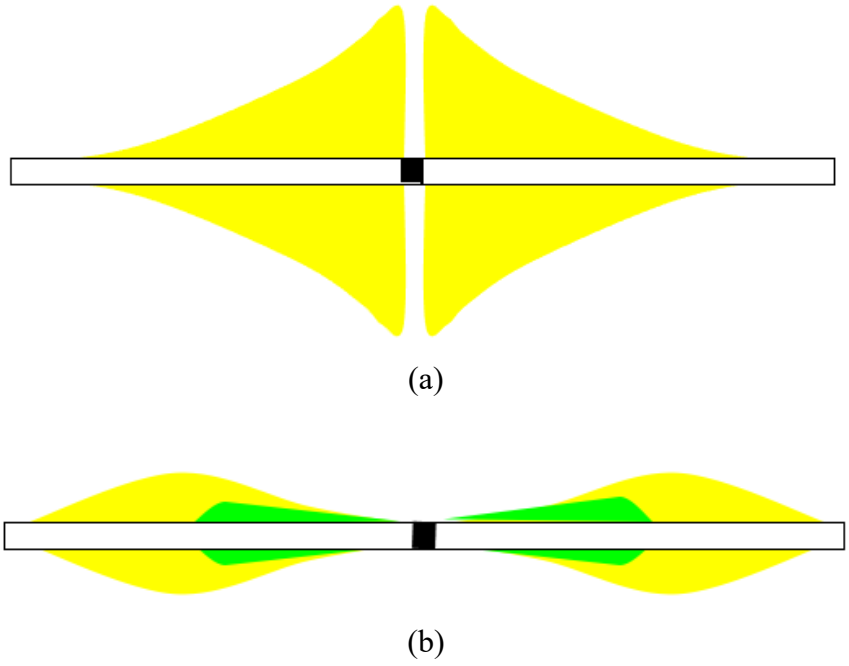

Figure 12. The schematic feature of photoelastic birefringence of shear stress around a fiber break of single glass fiber composites: (a) Without debonding and (b) With debonding

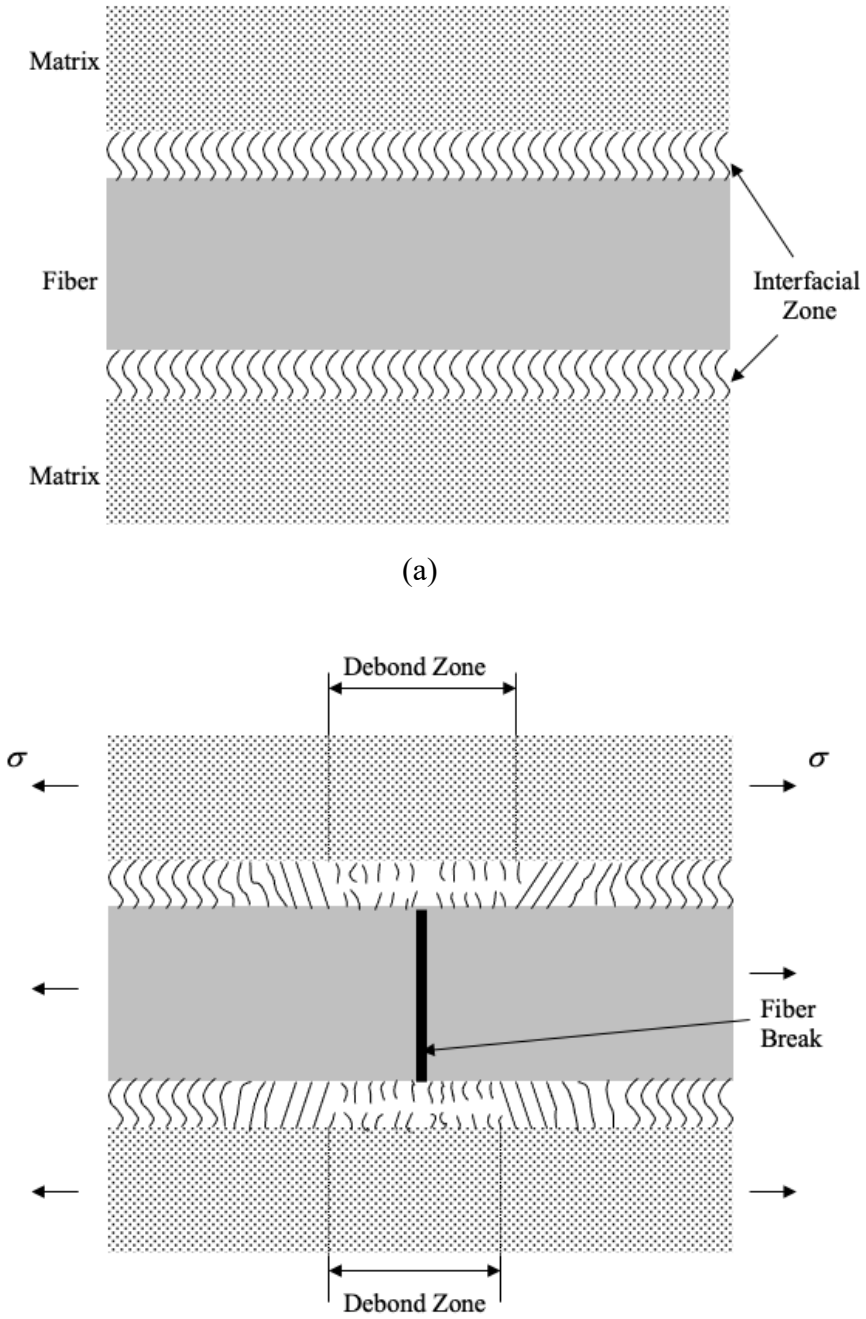

Figure 13. Schematic debonding microstructure of fiber and matrix interface. (a) Before loading (no fiber break), (b) After loading (fiber break).

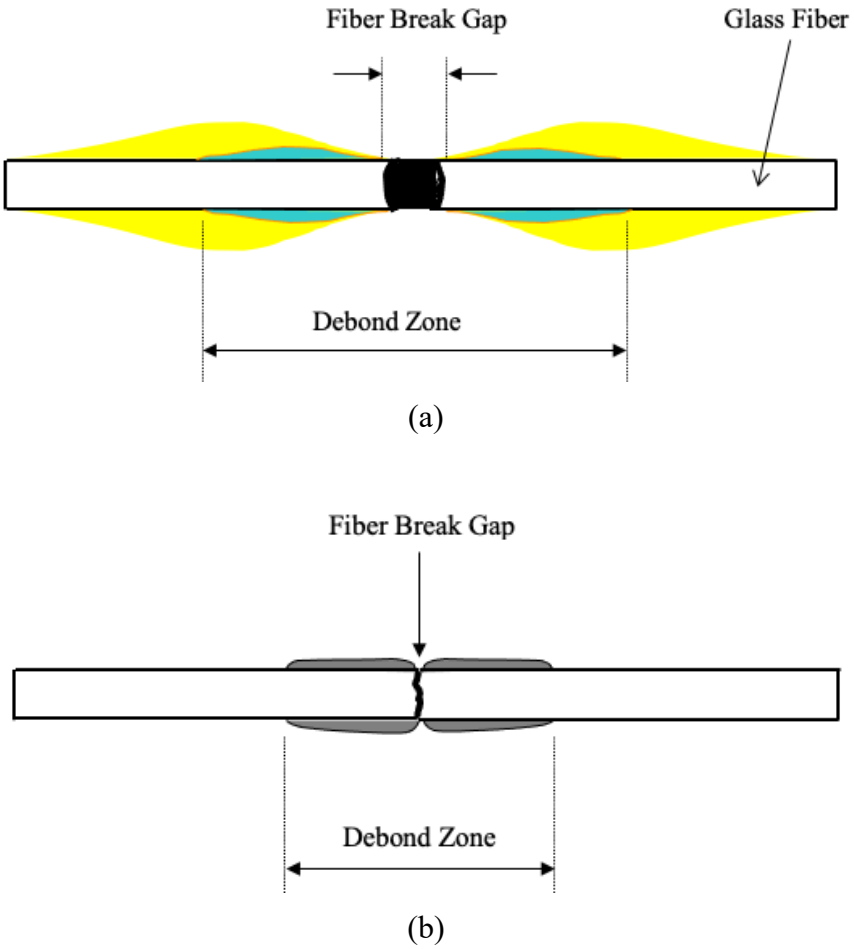

Figure 14. Schematic feature of debond zone of E-glass fiber. (a) Loading-applied state, (b) Loading-released state.

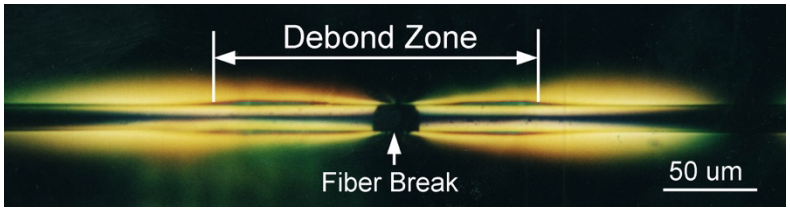

(a)

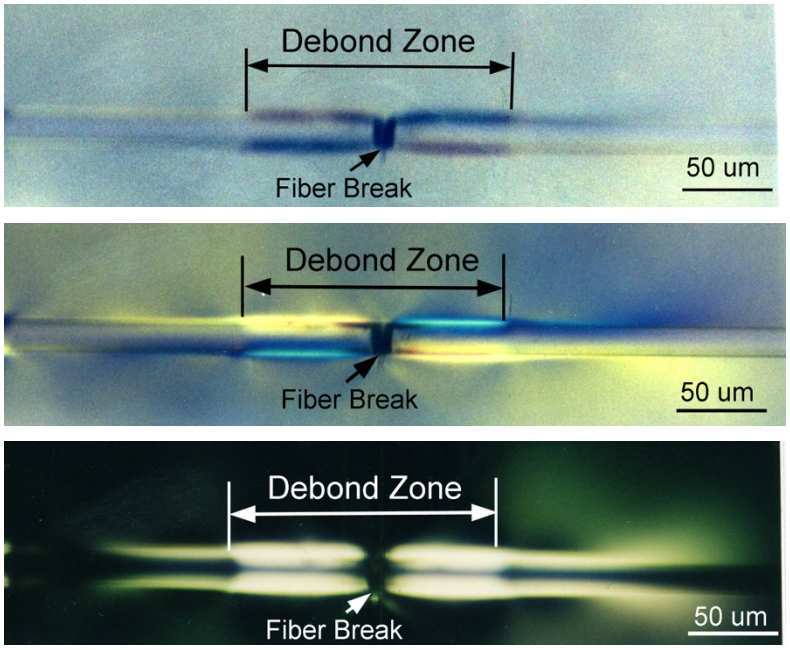

(b)

Figure 15. Measurement of debond zone of E-glass fiber. (a) Loading-applied state, (b) Loading-released state.

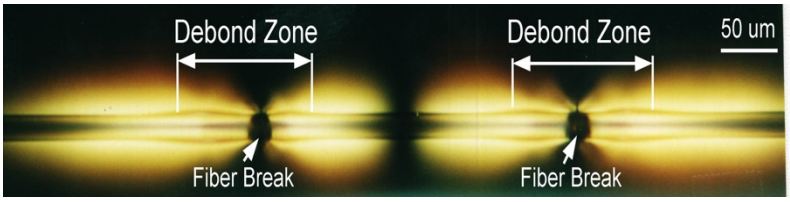

(a)

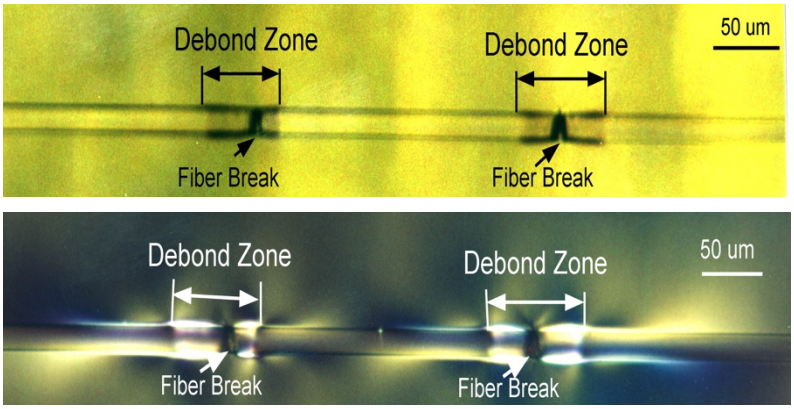

(b)

Figure 16. Measurement of debond zone of E-glass fiber. (a) Loading-applied state, (b) Loading-released state.

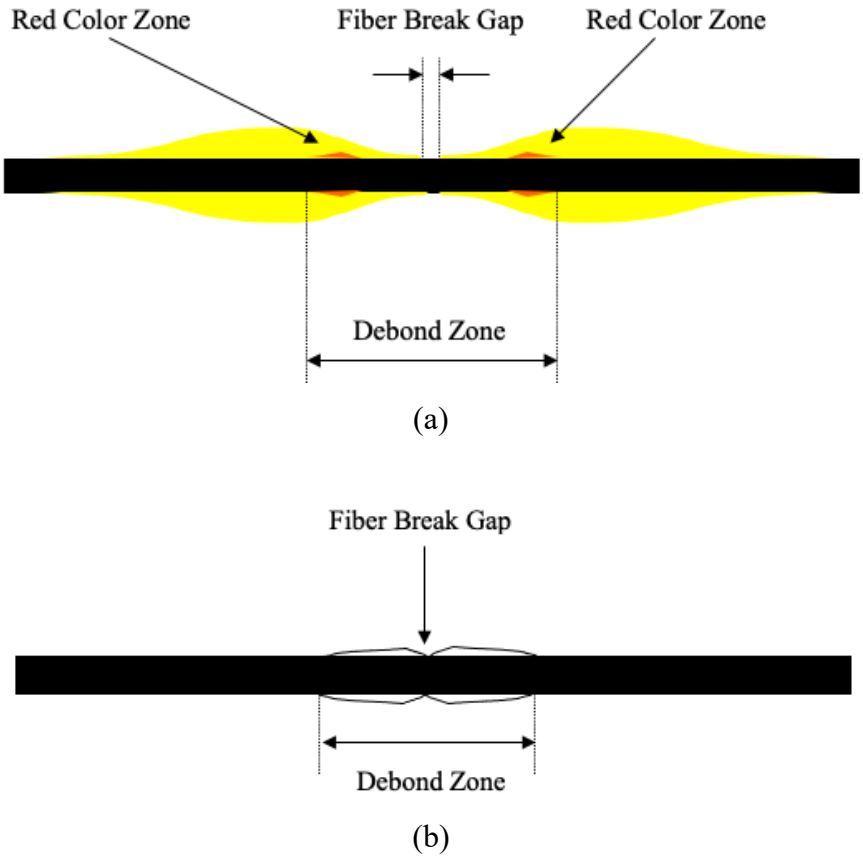

Figure 17. Schematic feature of debond zone of AS4 carbon fiber. (a) Loading-applied state, (b) Loading-released state.

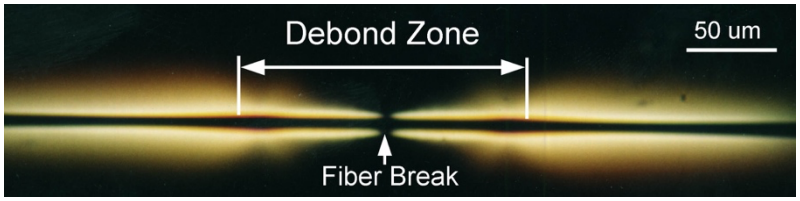

(a)

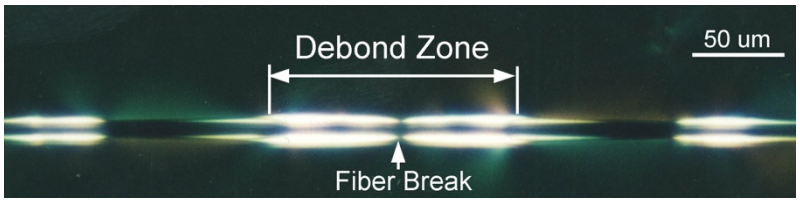

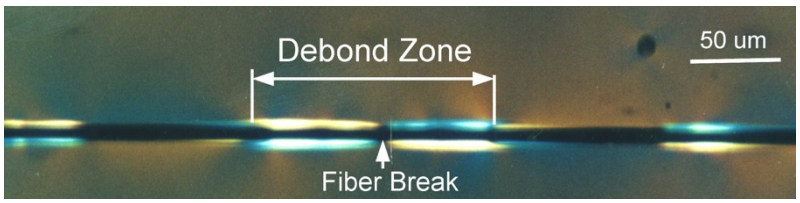

(b)

Figure 18. Measurement of debond zone of AS4 carbon fiber. (a) Loading-applied state, (b) Loading-released state.

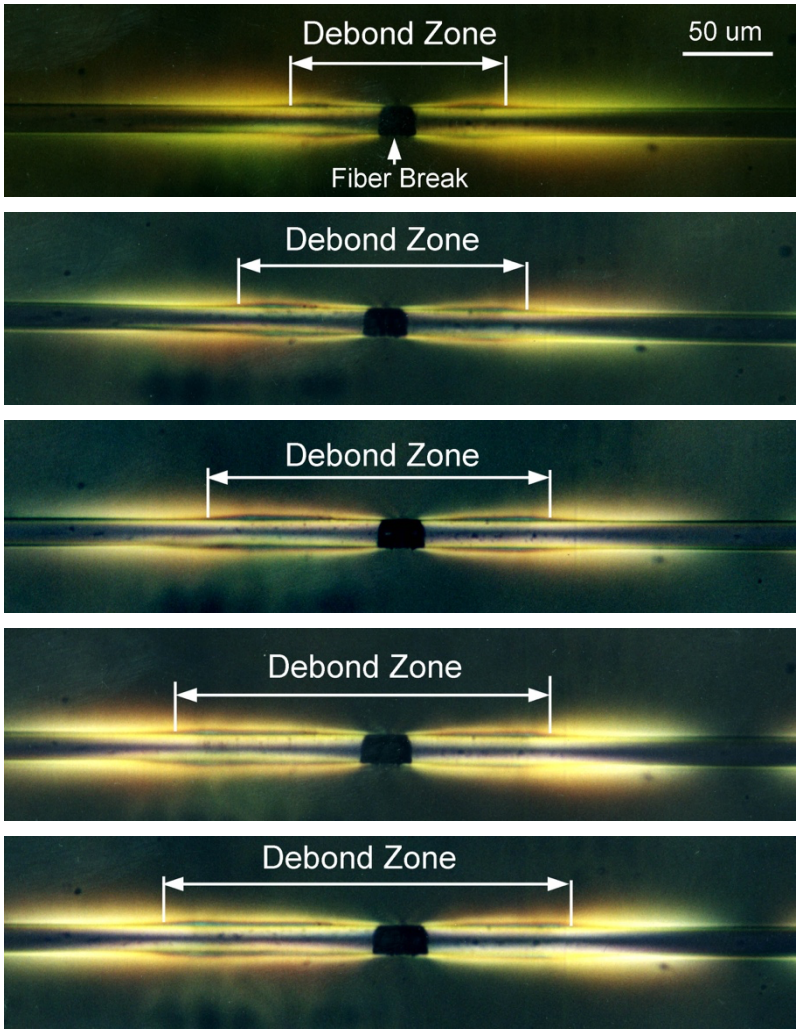

Figure 19. Debond growth of E-glass fiber against the applied stress.

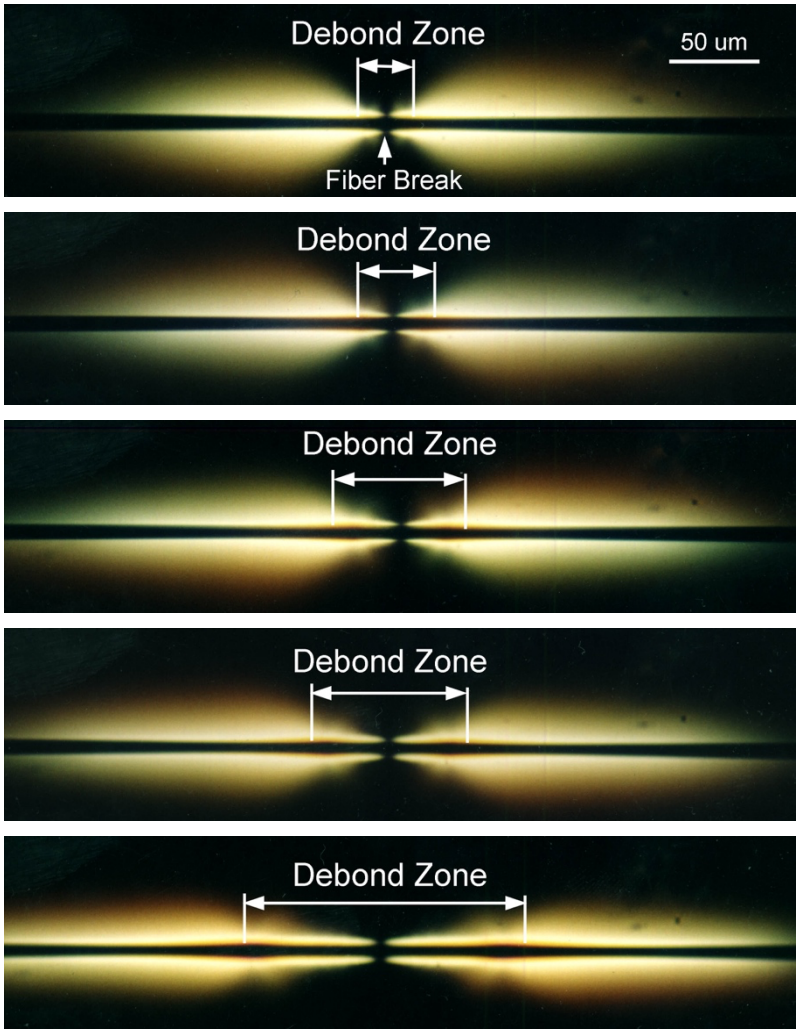

Figure 20. Debond growth of AS4 carbon fiber against the applied stress.

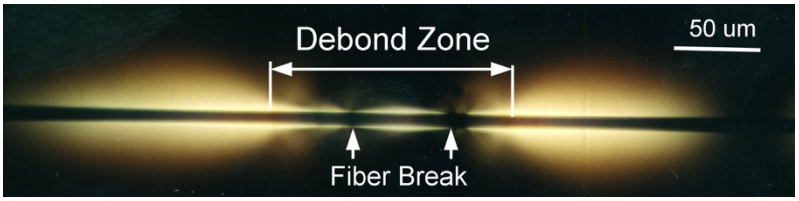

(a)

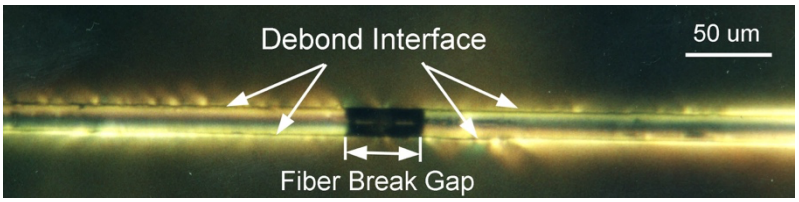

(b)

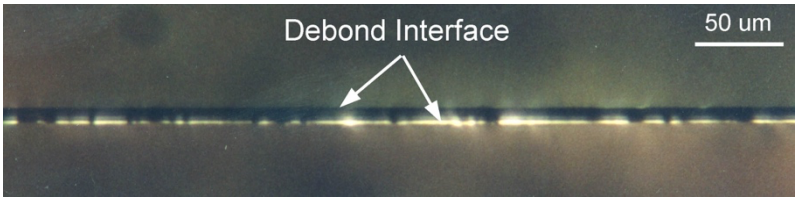

(c)

Figure 21. Examples of special debond zones of single fiber composites. (a) Connected debond zone (AS4 carbon fiber), (b) Very long debond done (E-glass fiber), (c) Debond interface without fiber break (AS4 carbon fiber).

(i) ε = 2.0 %:

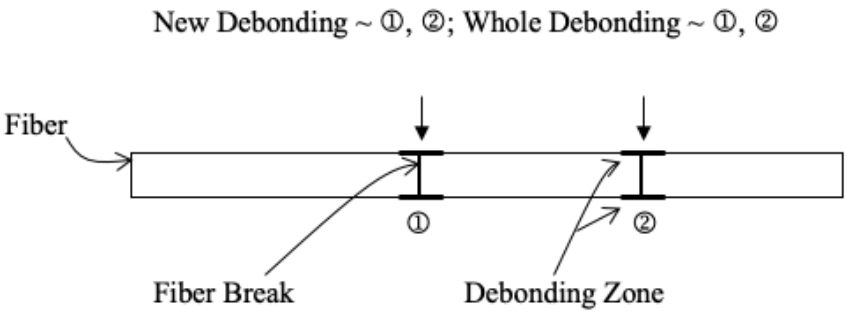

(ii) ε = 3.0 %:

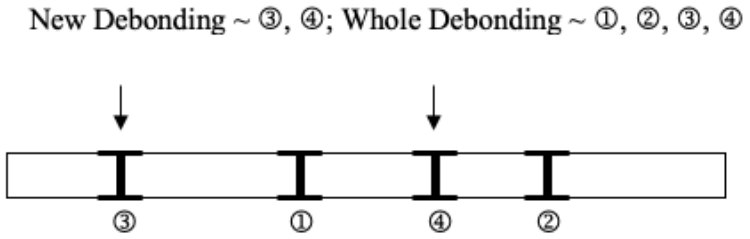

(iii) ε = 4.0 %:

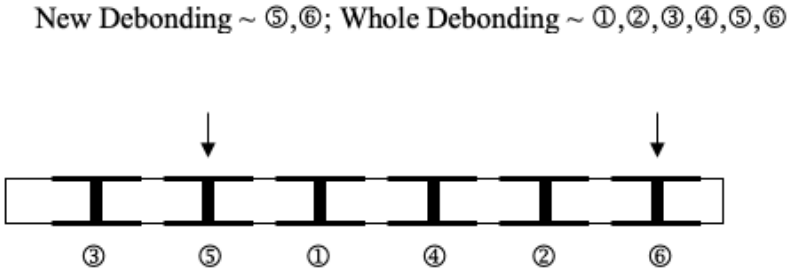

Figure 22. Schematic figures of instantaneous (new) debond zones and whole debond zones in single fiber composites.

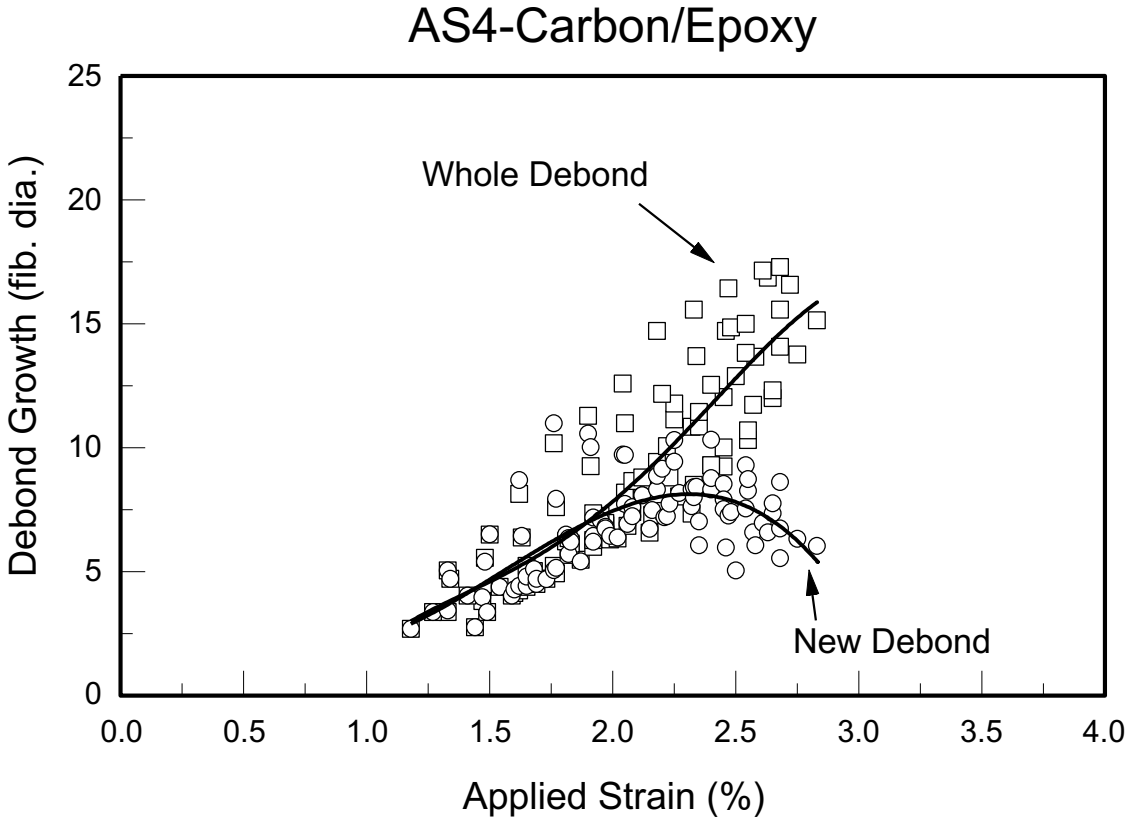

Figure 23. Instantaneous and whole debond lengths from AS4 carbon/epoxy composites. $\Gamma_{d,New\ Debond} = 220 J/m^2$. $\Gamma_{d,Whole\ Debond} = 130\ J/m^2$. ($r_f = 3.5\ \mu m$, $E_A = 231 GPa$, $\Gamma_f = 10\ J/m^2$).

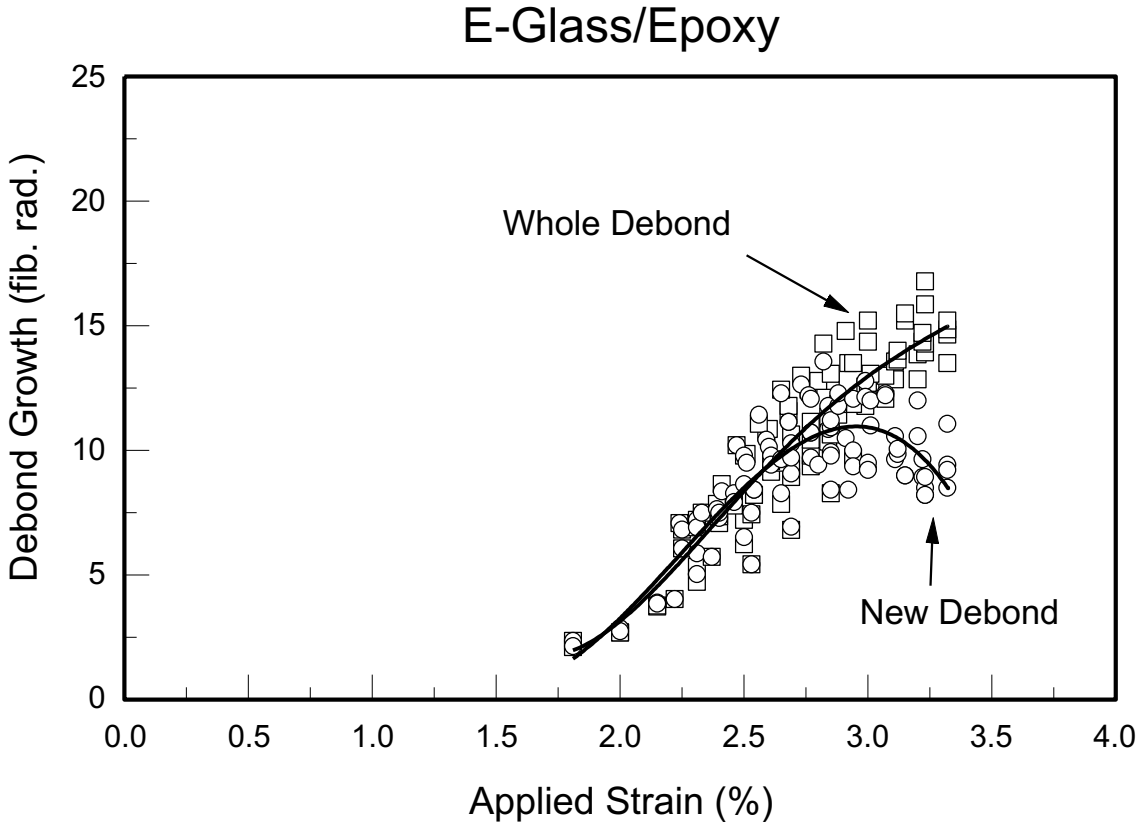

Figure 24. Instantaneous and whole debond lengths from E-glass/epoxy composites. $\Gamma_{d,\text{New Debond}} = 105$ J/m^2. $\Gamma_{d,\text{Whole Debond}} = 98$ J/m^2. (r_f=7.0 μm, E_A = 72.5 GPa, Γ_f = 10 J/m^2).

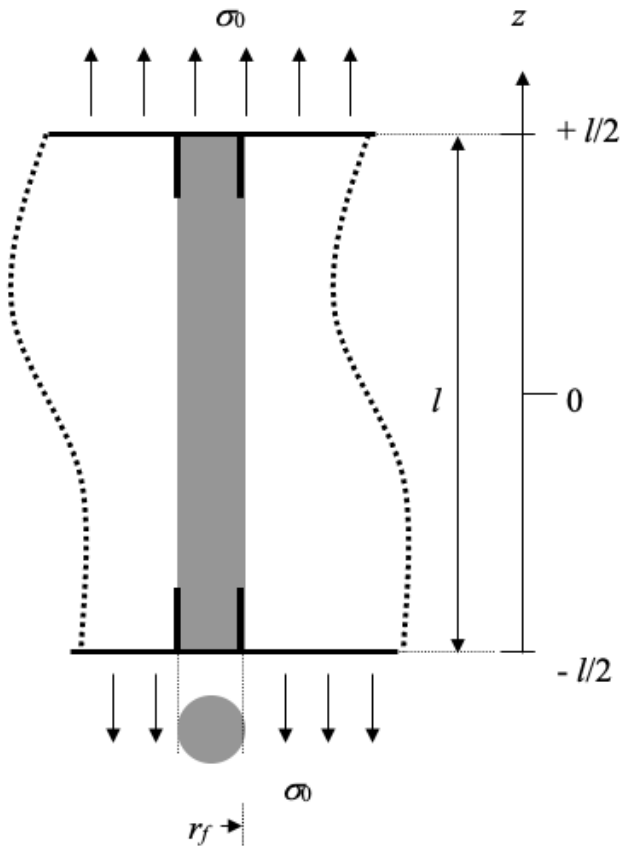

Figure 25. A single fiber fragment of length l and Radius r_f embedded in an infinite amount of matrix.